TECHNICAL RESEARCH REPORT

SYSTEMS RESEARCH CENTER

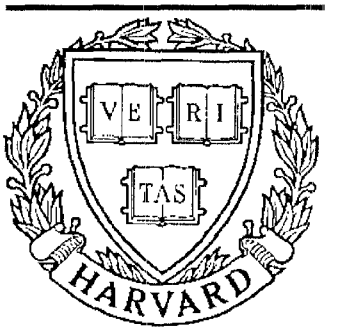

Supported by the National Science Foundation Engineering Research Center Program (NSFD CD 8803012), Industry and the University

Organization of Response Areas in Ferret Primary Auditory Cortex

by S.A. Shamma, J.W. Fleshman, P.R. Wiser, and H. Versnel

TR 92-105

ORGANIZATION OF RESPONSE AREAS IN FERRET PRIMARY AUDITORY CORTEX

Shihab A. Shamma[a], *James W. Fleshman*[b], *Philip R. Wiser*[c], *and Huib Versnel*[c]

(a) Electrical Engineering Department, University of Maryland Institute for Advanced Computer Studies, and Systems Research Center. University of Maryland, College Park, MD 20742. The Mathematical Research Branch, NIDDK, National Institutes of Health, Bethesda, MD 20892.

(b) Systems Research Center, University of Maryland, College Park, MD 20742. *Present Address:* National Center for Biotechnology Information, National Library of Medicine, Bethesda, MD 20894.

(c) Electrical Engineering Department and Systems Research Center, University of Maryland, College Park, MD 20742.

ABSTRACT

We studied the topographic organization of the response areas obtained from single- and multi-unit recordings along the isofrequency planes of the primary auditory cortex (AI) in the barbiturate-anesthetized ferret. Using a two-tone stimulus, the excitatory and inhibitory portions of the response areas were determined and then parameterized in terms of an *asymmetry index*. The index measures the balance of excitatory and inhibitory influences around the best frequency (BF). The sensitivity of responses to the direction of a frequency-modulated (FM) tone was tested and found to correlate strongly with the asymmetry index of the response areas. Specifically, cells with strong inhibition from frequencies above (below) the BF preferred upward (downward) sweeps. Responses to spectrally shaped noise were also consistent with the asymmetry of the response areas: cells that were strongly inhibited by frequencies higher than the BF responded best to stimuli that contained least spectral energy above the BF. In a local region, most cells exhibited similar response area types and other response features. The distribution of the asymmetry index values along the isofrequency planes revealed systematic changes in the symmetry of the response areas. At the center, response areas with narrow and symmetric inhibitory sidebands predominated. These gave way to asymmetric inhibition, with high frequency inhibition (relative to the BF) becoming more effective caudally, and low frequency inhibition more effective rostrally. These response types tended to cluster along repeated bands that paralleled the tonotopic axis. One functional implication of the response area organization is that cortical responses encode the locally averaged *gradient* of the acoustic spectrum by their differential distribution along the isofrequency planes. This enhances the representation of such features as the symmetry of spectral peaks, edges, and the spectral envelope. This scheme can be viewed as the one-dimensional analogue of spatial phase sensitivity in simple cells of the primary visual cortex, which there gives rise to spatial frequency channels and orientation columns.

INTRODUCTION

The mammalian primary auditory cortex, AI, plays an important role in localizing and processing complex sounds (*Brugge et al. 1969*; *Evans and Whitfield 1964*; *Jenkins and Merzenich 1984*; *Neff et al. 1975*; *Suga 1984*; *Whitfield 1980*). Despite extensive neurophysiological and anatomical study, the organizational principles underlying cortical auditory function, and the primitives that the AI employs to represent sound remain poorly understood. Only two general organizational principles have been identified in AI: first, frequency is mapped in an orderly fashion across the surface of AI (the tonotopic axis) (*Kelly et al. 1986*; *Merzenich et al. 1975*; *Merzenich et al. 1976*; *Reale and Imig 1980*); second, cells with similar responses to binaural stimuli tend to occupy irregular bands that are oriented parallel to the tonotopic axis and, therefore, approximately orthogonal to the isofrequency contours (*Imig and Adrian 1977*; *Middlebrooks et al. 1980*; *Wenstrup et al. 1986*). Such superimposed response maps also exist in other primary sensory cortices as, for instance, in the retinotopic map and the ocular dominance columns of the visual cortex (*Hubel and Wiesel 1968*). In the visual cortex maps have also been found for other image attributes such as selectivity to spatial frequencies, edge orientations, and direction of motion (*Hubel and Wiesel 1962*; *Zeki and Shipp 1988*; *de Valois and de Valois 1988*). Corresponding ordered representations of complex spectral or temporal attributes of sound have not been identified in the auditory cortex of mammals, except in the echo-locating bat (*Suga 1977*; *Suga and O'Neill 1979*; *Suga and Manabe 1982*). Recent data from cat's primary auditory cortex, however, have suggested a possible organization of FM sensitivity along the isofrequency planes (*Mendelson et al. 1988*).

The aim of this study was to determine whether features of the acoustic spectrum other than frequency and binaurality are represented topographically across the ferret AI. To do so, we examined the organization of the excitatory and inhibitory response areas in single- and

multi-unit clusters. Our specific goal was to establish whether systematic changes occur in these response areas as a function of position along the isofrequency contours. If so, it may be possible to determine what spectral features of the stimulus those changes represented and their functional significance.

METHODS

Surgery and animal preparation

Data presented here were derived from experiments with 50 ferrets, *Mustela putorius*, supplied by the *Marshal Farms*, Rochester, NY. Young adult ferrets (approximately 1 kg) were anesthetized with sodium pentobarbital (40 mg/kg, intraperitoneal) and given 0.1 mg/kg Atropine subcutaneously. An areflexic level of anesthesia was maintained throughout the surgical preparation and subsequent neural recording session by continuous intravenous infusion of pentobarbital (approximately 5 mg/kg/hr) diluted with dextrose-electrolyte solution to maintain the animal hydration and to provide nourishment. In our experience, nutrition during the experiment was essential to keep the animals in good condition for prolonged recording periods up to 36 hours. A tracheal cannula was inserted and breathing was unassisted. Body temperature was maintained near 38°C using a heating pad and blankets. The ectosylvian gyrus, which includes the primary auditory cortex (*Kavanagh and Kelly 1987*; *Kelly et al. 1986*), was exposed by craniotomy and the overlying dura was incised and reflected. The brain was covered in 2% agar in saline to reduce pulsations. The contralateral pinna and most of the fleshy meatus were resected. The ear canal was cleaned, and a speculum containing a Sony MDR-E464 miniature speaker was sutured to the meatal stump. The speculum is cone-shaped, tapering from a diameter of 20 mm to 2.5 mm, and is 15 mm long. An experiment was concluded with an overdose of pentobarbital after 12-36 hours of recordings.

Acoustic stimuli

Pure tone stimuli (single and two-tone bursts, 200 ms duration, 10 ms rise- and fall-times, 0–50 ms intertone delay) and FM sounds (10 ms rise-fall times, 500 ms duration) were generated using two independent function generators, gated and mixed, and then fed through a common

equalizer into the earphone. Other parameters of the test stimuli are described in RESULTS. Noise bursts (200 ms duration, 10 ms rise- and fall-times) were also used in some experiments. Before gating and delivery, they were spectrally shaped by an independent computer-controlled equalizer with 1/3 octave resolution. With this resolution, the narrowest band of noise that could be generated was just under 2/3 octaves, and the slopes of the noise band edges were approximately 60 dB/octave. Calibration of the sound delivery system (up to 20 kHz) was performed *in situ* prior to each experiment using a 1/8 inch Brüel & Kjaer probe microphone (type 4170). The microphone was inserted into the ear canal through the wall of the speculum to within 5 mm of the tympanic membrane. The speculum and microphone setup resembles closely that suggested by Evans (1979). The signal from the microphone is then fed into an amplifier and a narrow bandpass filter. An automatic calibration procedure is then performed where at each frequency, the level of the signal is increased until the microphone output equals a predetermined level corresponding to 84 dB SPL. The absolute calibration reference is obtained independently using a Brüel & Kjaer Calibrator (type 4230) at 1 kHz. Maximum tone intensities used were limited to 85 dB SPL to ensure the linearity of our acoustic delivery system.

Recordings

Action potentials from multi-unit clusters and single units were recorded using glass-insulated tungsten microelectrodes with 5-6 $M\Omega$ tip impedances. Neural signals were led through a window discriminator and the time of spike occurrence relative to stimulus delivery was stored using a Hewlett-Packard 9000/800 series minicomputer. The computer also controlled stimulus delivery, and created raster displays and spike count histograms of the responses.

In each animal, electrode penetrations were made orthogonal to the cortical surface. Our strategy was to maximize the number of such penetrations along the isofrequency planes. This necessarily limited the number of stimulus parameters tested in a given penetration. An experiment typically consisted of 10–40 useful microelectrode penetrations spaced 100–300 μm apart. In each penetration, 1–9 cells or cell clusters were studied. In all recordings of clusters, the evoked potential was always filtered out prior to triggering, and the trigger level was set at a high enough level to accept the largest spikes. In several penetrations, responses were

recorded at various depths to measure variations as a function of depth. The frequency range tested in a given animal was often dictated by the available cortical surface not obstructed by superficial blood vessels.

In all mapping experiments, recordings were made at a depth of 350-600 μm. Excitatory phasic responses to single tones at this depth are strongest. Histological examination of Nissl-stained sections showed that this depth corresponds to cortical layers III and IV in young adult ferrets. In a few experiments where columnar organization was studied, recordings ranged from 150 μm to 750 μm in depth. For each cell or cell cluster, we first determined the best frequency (BF) manually, followed by a tuning curve with up to 1/8 octave resolution at near threshold intensity. BF was defined to be the frequency of the lowest threshold. Determining the BF accurately was important, especially in cases where the tuning was broad at the moderate sound intensities used in the two-tone tests.

Single-unit and multi-unit recordings

Cortical units are rather small and difficult to isolate and hold individually for long periods. Consequently, we most often opted to record spikes from cell clusters (2-5 cells) rather than single cells in order to map a large cortical area in reasonable time. In such multi-unit recordings, one cannot be certain that the number of events detected corresponds exactly to the number of spikes present. To avoid ambiguity, we shall strictly distinguish the two types of records in our figures and discussion by using the term **response amplitude** to signify the number of events recorded in multi-unit records. The term **spike count** will be reserved for single-unit records only.

A note on terminology

In general, responses of cortical cells represent the final outcome of a complex series of transformations at all pre-cortical nuclei and structures. This causes certain difficulties in the choice of appropriate terms to interpret the responses. For instance, our two-tone paradigm cannot distinguish between inhibitory responses due to neural processes at various auditory nuclei, and suppression due to basilar-membrane mechanics. Thus, to simplify the remainder of this text, we shall not differentiate between these two processes and shall use the term

inhibition to refer to their net effect at the cortex.

Another term which is frequently used here is the **response area** of a cell or cluster. It is used to denote the response as a function of a tone's frequency and intensity. In some of our data, the response area of a cell or cluster is fully determined. In many cases, however, the response is obtained only at one or a few intensities. When discussing the latter data, the context should make it clear that reference is made only to specific slices of the response area.

Data analysis

Responses described in this report were obtained from single- and multi-unit recordings in the AI. In each recording, the BF was measured, together with the response area of the cell or cluster and its response to various FM sweeps and noise stimuli. The response area was determined using the two-tone stimulus depicted in Fig. 1 (*Suga 1965a*). It consisted of two tone bursts of equal duration with staggered onset times as illustrated in Fig. 1A. The tone burst ($T1$) was presented at several different frequencies centered around the BF of the cell to measure the excitatory response area (top raster in Fig. 1A). Since many cells exhibit low spontaneous firing rates, partly because of the depression of spontaneous activity by the anesthetic used in these experiments (*Brugge and Merzenich 1973*; *Pfingst and O'Connor 1981*), it was difficult to see the inhibitory portions of the response area using a single tone. Therefore, a tone burst ($T2$) was fixed at BF, with a delay of 0–50 ms relative to $T1$, to provide a level of background activity against which the inhibitory response area could be measured (bottom two rasters in Fig. 1A). For most recordings, the inter-tone delay was chosen at 25 ms. This value provided a good visual compromise between adequate segregation of the phasic responses (to facilitate the computations of the response amplitude curves) and visual grouping of the responses to allow for easy inspection of their properties.

Response amplitude curves as a function of frequency are counted directly from the two-tone rasters (Fig. 1B). Intervals over which the counts are made are indicated by the bold arrows along the time axis of the two-tone rasters. The solid curve represents the excitatory phasic responses to $T1$. The dashed curve is the count from the slightly delayed phasic responses to $T2$. Depression of response counts in this latter curve reflects the inhibitory influences due

to $T1$. Repeating these measurements at various $T1$ intensities, the response area of a cell or cluster could be determined.

An important descriptive feature of the response area of a given cell or cluster is the symmetry of its inhibitory and excitatory portions around the BF. To parametrize this feature, we first define the *total response amplitude curve* (Fig. 1C) as the sum of the two curves in Fig. 1B, i.e., the combined count from the phasic responses to both $T1$ and $T2$. This curve represents the total excitatory and inhibitory responses around the BF. To indicate the symmetry of this curve about the BF, we compute the following simple statistic:

$$M = \frac{R_{>BF} - R_{<BF}}{R_{>BF} + R_{<BF}}, \tag{1}$$

where $R_{>BF}$ and $R_{<BF}$ are the total number of spikes (or response amplitude) for an equal number of frequencies above and below the BF, respectively; the count at BF is not used in this measure. If the excitatory and inhibitory responses are approximately symmetric around BF, the measure (M) will be near zero. Inhibition of $T2$ responses by $T1$ stimuli above BF and/or spread of $T1$ excitation to lower frequencies ($< BF$) causes M to be negative. Conversely, stronger low frequency inhibition or high frequency $T1$ excitation produces positive M values. Note that the M index as defined above is computed at one $T1$ intensity. To characterize the entire response area of a cell or a cluster, the index is computed at each intensity, and then averaged over all $T1$ intensities used. Similarly, to characterize a given penetration which contain several cells or clusters, the index M is averaged over all tests.

FM tones were presented in two sweep directions, and at different rates and intensities as discussed later in the text. The symmetry of the average responses to the two sweep directions was assessed using the index C as follows:

$$C = \frac{R\uparrow - R\downarrow}{R\uparrow + R\downarrow}, \tag{2}$$

where $R\uparrow$ and $R\downarrow$ are the response amplitudes to the up and down sweeps, respectively.

In the case of the noise stimuli, only three spectrally-shaped bursts were used. One was narrowband ($< 2/3$ octaves) placed symmetrically about the BF. The response to this stimulus provided the reference against which the responses to two other asymmetric noise bands were

compared. The asymmetric stimuli had spectral noise energy that extended up to an octave above BF in one case, and down to an octave below BF in the other. The asymmetry index used in this case is defined as:

$$S = \frac{R_{>BF} - R_{<BF}}{R_{>BF} + R_{BF} + R_{<BF}} \tag{3}$$

where $R_{>BF}$, R_{BF}, $R_{<BF}$ are the response amplitude to each of the three noise bands. Note that this index is identical to M except for the extra normalization by the count at BF (R_{BF}). Without it, the index S becomes too sensitive when both $R_{>BF}$ and $R_{<BF}$ are small. This is not a problem with index M since many frequencies are tested about the BF, and hence $R_{>BF} + R_{<BF}$ is never too small.

Topographic representation of the data

The primary objective of the experiments reported here is to determine the topographic distribution of the M, C, and S index values across the surface of AI. In the ferret, AI is located on the ectosylvian gyrus (*Kavanagh and Kelly 1987*; *Kelly et al. 1986*). As in the cat, its exact location, orientation, and particularly its width, varies from one animal to another. On average, AI occupies the dorsomedial-most 3-4 mm of the ectosylvian gyrus, extending into the supra-sylvian fissure. AI widens from 1-2 mm in the lower BF regions, to 3-4 mm at higher BFs.

To determine roughly the location and tonotopic organization of AI, it was generally necessary during the mapping experiments to make several initial exploratory penetrations. The physiological criteria by which the ferret AI responses are recognized are similar to those described in the cat (*Abeles and Goldstein 1972*; *Kelly et al. 1986*; *Phillips et al. 1985*). They are strong, phasic, relatively sharply tuned, and have a short latency (15-20 ms) (*Fleshman and Shamma 1988*). In each animal, the M, S, and/or C indices were determined for numerous penetrations distributed across the AI, and displayed using an arbitrary classification scheme. In this scheme, M values outside of the range of values ± 0.07 are considered highly asymmetric, while M values in the range ± 0.03 are considered symmetric. A comparable proportion of the total number of penetrations was represented in each class (roughly 50-80 penetrations).

Similar procedures were applied in representing the S and C indices. The resulting maps for each animal show the topographic distribution of index values, together with the supra-sylvian fissure and a few schematic isofrequency lines.

RESULTS

Data illustrated here were collected from over 400 penetrations in the AI of 50 ferrets. In all recordings, a measure of the response area of the cell or cluster was obtained using the two-tone stimulus. In a large proportion of the recordings, responses to noise bursts and FM tones were also recorded. In the following, we first describe the primary response feature of interest in this study, that of categorizing the response areas based on their symmetry. We then discuss the corresponding response patterns evoked by FM and noise stimuli. Finally, we examine the topographic distribution of these responses across the surface of AI.

Since all but one of these maps were obtained using multi-unit records, our description of the response area types and other response features will mostly utilize these types of recordings. However, the correspondence between single- and multi-unit records in our experimental paradigm is explored in some detail. Furthermore, single-unit recordings are used to demonstrate a columnar organization in AI.

Symmetry of response areas

Response areas in AI vary widely in the extent, efficacy, and detailed shape of their inhibitory and excitatory portions. Nevertheless, they can be broadly grouped into three types based on their symmetry (Fig. 2): symmetric (column **I**) and asymmetric responses (columns **II** and **III**). In column **I**, the excitatory response of the symmetric cluster is sharply tuned at $BF = 8.5$ kHz. $T1$ inhibits the response to $T2$ over a broader range on either side of BF (approximately 6–12 kHz). Two regions of $T2$ inhibition can be distinguished. The first region is at frequencies where $T1$ is excitatory, i.e., within the narrow tuning curve of the response. The second region is at frequencies where $T1$ elicits little or no response, i.e., the so-called side-bands of the tuning curve. This region is marked by arrows in the rasters. Response areas with such inhibitory responses are said to exhibit lateral inhibition. The total response amplitude curve in this case has symmetric dips about the BF (Fig. 2C, column **I**).

A response with an asymmetric pattern of inhibition is shown in column **II**. Its BF is at 3.5 kHz. However, in contrast to the earlier response, the inhibition due to T1 is nearly one-sided, being relatively strong below the BF, and weak above the BF. Therefore, its total response amplitude curve (Fig. 2C, column **II**) has a larger dip below the BF.

The raster response in column **III** exhibits the opposite asymmetry. Once again, the excitatory responses to T1 are well tuned (BF = 8.0 kHz). The inhibitory influences of T1 are stronger here above the BF. Hence its total response amplitude curve (Fig. 4C, column **III**) is asymmetric with a large dip above the BF.

The apparent symmetry or asymmetry of the above response patterns can be captured by the asymmetry index M as defined in METHODS. For the symmetric responses in column **I**, M is near zero (M = 0.02). The index is positive when inhibition is strongest below the BF (M = 0.23 in column **II**), and is negative when the inhibition is strongest above the BF (M = –0.21 in column **III**).

Variability of response areas

The three response types illustrated in Fig. 2 are typical in that they exemplify the majority of recorded cells and clusters. A significant range of variations, however, exists in the character of the responses observed within each of the three types. For instance, three variants of each response type are displayed in Fig. 3. In column **I**, the responses exhibit stronger and broader side-band inhibition ($\geq \pm 1$ octave around the BF) than that typically found around the BF (approximately $\pm 1/2$ octave as in Fig. 2A, columns **I** and **III**).

In column **II**, the responses exhibit side-band inhibition that is somewhat weaker and narrower in extent. Such side-bands do not necessarily imply broader excitatory tuning around the BF (e.g., top and bottom rasters). In fact, it is common for well tuned symmetric responses (top raster) to be accompanied by very narrow side-band inhibition that is difficult to detect.

In column **III**, lateral inhibition is weakest. In such cases, a gradual overlap of the $T1$ and $T2$ responses results in shallow total response curves over all frequencies. In the asymmetric cases (bottom two rasters), and especially for negative M values, the weak side-band inhibition is typically accompanied by a considerable spread of the excitatory responses to $T1$ (see also

middle raster of column **II**).

In all response patterns illustrated so far, specific choices were made of stimulus parameters such as the inter-tone delays (= 25 ms) and $T1$ and $T2$ intensity levels. Changing these parameters for a given record affects somewhat the absolute values of the M, but rarely changes the response type, e.g., changing M from a large positive to large negative values, or vice versa. Figure 4 illustrates the stability of the responses for two out of 20 cells that were tested with decreasing inter-tone delays. In the top row, the cell maintained a strong inhibition above the BF for all delays tested. In the bottom row, the inhibition was mostly below the BF.

The same observations hold for the choices of the intensity levels. In the ferret, the lowest response thresholds that we observed are around 30 dB SPL, and more typically somewhat higher (40-50 dB SPL). As a rule, the intensity of the $T2$ (BF) tone was always chosen to provide an adequate background of responses against which inhibition could be detected (usually at 60–70 dB SPL). T1 tone levels spanned a wide range of intensities around the T2 level, from threshold up to 85 dB SPL. The most common change that occurs when increasing the T1 level relative to T2 is for negative (positive) M values to become more negative (positive). Equivalently, the asymmetry of the response area of a cell becomes more accentuated at higher relative $T1$ levels. Changes of M index sign occur almost exclusively in the near symmetric penetrations. Examples of response areas from three single units measured over 30 dB change in $T1$ intensities are shown in Fig. 5. The thresholds of the excitatory and inhibitory portions of these response areas were measured from the two-tone raster recorded at each T1 level as described in METHODS and Fig. 1. In Fig. 5A, the cell is narrowly tuned around 7.5 kHz and the inhibition of $T2$ responses mostly overlaps with the excitatory responses to $T1$. In contrast, the inhibitory response area for the cell in Fig. 5B spreads extensively and asymmetrically below the BF. The opposite occurs in Fig. 5C.

Columnar organization of response area types

The origin of the variability in response area shapes (e.g., Fig. 3) is uncertain. It may, for instance, reflect the diversity of cortical cell types and morphologies throughout the different cortical layers. Our records are restricted to intermediate depths, and from cells/clusters that

are excitatorily and phasically driven by single tones at BF. Within this group of cells in a given penetration, there seems to be no significant variability in the overall organization of the response areas, e.g., the symmetry of the inhibition.

This columnar organization of the response areas is illustrated in Fig. 6A. In each series of recordings, an electrode penetration was made orthogonal to the surface of AI, and single units were isolated at various depths. In series **I**, all cells exhibited relatively strong inhibition above the BF. In series **II**, the response areas were symmetric. In series **III**, the response areas exhibited broader inhibition below the BF. Such results were obtained from 66 single units in 16 electrode tracks. These data are quantitatively summarized in the plots of Fig. 6B. The left panel illustrates the distribution of M indices from all these units (SD = 0.20). In this sample, the mean asymmetry index was -0.05, 30% of the cells were symmetric, 29% had stronger low-frequency inhibition, and 41% exhibited stronger high-frequency sideband inhibition. For comparison, the right panel shows the distribution of the *deviation* of the M index of each unit from the average index value of its penetration. It is evident that the latter distribution is narrower (SD = 0.13), implying a dependence between the index of a penetration and the single units within it, and hence the existence of a columnar organization. On average, 52% of units encountered in a given penetration are within ± 0.07 of the average index value, and over 65% are within ± 0.1. Consequently, it is unlikely to encounter units of extreme opposite asymmetries in the same penetration.

Correspondence between single-unit and multi-unit recordings

Another possible source of variability in the response area shapes is the use of cluster records. To assess the importance of this factor, we obtained 45 combined cluster and single unit recordings at the same location so as to compare the two types of records. The basic finding illustrated by the raster responses in Fig. 7A is that the character of the response areas of a cluster and its nearby single units are very similar. This is demonstrated again in Fig. 7B using the data from all records (45 clusters and 61 associated single units). The M index value of each cluster is plotted against that of 1-3 single units isolated from the same trace. Linear regression analysis indicates a significant correlation in the value of the indices obtained from

both records. Thus, except near the origin where response areas are symmetric, indices have the same signs, reflecting consistent response area types from both records. Note also that the spread in the single-unit indices is larger than that of the clusters.

Responses to FM tones

One possible consequence of the asymmetry in the response area of a cell is its sensitivity to the direction of an FM stimulus. Such a property cannot be easily deduced from the two-tone stimulus because of its essentially stationary nature. In order to test this hypothesis directly, FM tones were swept up and down past the BF of the cells/clusters, spanning a total frequency range of ± 1 octave, and presented at different rates, most often at 10, 30, and 50 kHz/s (see bottom of Fig. 8A for an illustration of stimulus parameters). The symmetry of the average responses to the two sweep directions were assessed using the index C (as described in METHODS).

In a total of 110 cells or clusters both FM and two-tone stimuli were presented. In approximately 80% of all cases, there is agreement between the response type of the two stimuli, i.e., responses with relatively strong inhibition above (below) the BF prefer upward (downward) sweeping tones. Symmetric cells respond well to both FM directions. Figure 8A illustrates the correspondence between two-tone and FM raster responses of upward, bidirectional, and downward-sensitive cells (from left to right). In Fig. 8B, this correspondence is quantified in terms of the asymmetry and directional sensitivity indices (M and C, respectively) computed from the responses of 46 multi-unit clusters in 5 experiments. The two indices are significantly correlated ($P < 0.001$). Finally note that, with few exceptions that occur in the near symmetric responses, FM directional sensitivity does not depend on sweep rate (Fig. 8A). However, the strength of the responses does vary with sweep rate. Some cells/clusters respond well only at faster rates, while others only at slow or intermediate rates.

Responses to spectrally shaped noise stimuli

In six animals, an additional stimulus paradigm was used to assess asymmetry in the response area above and below BF. The stimuli were three spectrally shaped noise bursts (Fig. 9). One stimulus was narrowband ($< 2/3$ octaves) placed symmetrically about the BF of the cell.

The response to this stimulus provided the reference against which the responses to the other two asymmetric bands were compared. For each recording, the asymmetry index, S, was computed from the responses as described in METHODS.

In approximately 70% of all cases, the responses obtained from the shaped noise is consistent with the asymmetry of the response area as measured with the two-tone stimulus. Figure 9 illustrates this correspondence for three different response area types. In the left rasters, the inhibition is below the BF, and hence the most effective noise stimulus is the one that has no energy below the BF (S=0.15). The opposite is true in the right rasters (S= –0.14). In the middle rasters, lateral inhibition is strong, and the responses are consequently stronger for the narrow band stimulus (S=0.03).

The topographic distribution of response area types

We examined the spatial distribution of response area asymmetry, as reflected in the M index, along the isofrequency contours of the primary auditory cortex in 24 animals. Frequencies represented in ferret AI range from 100 Hz to over 35 kHz, with the best responses at 5-8 kHz. A typical layout of the AI isofrequency contours is shown in Fig. 10. Note that on the rostro-medial edge of AI, BFs approach 20-25 kHz and then reverse their upward trend and begin to decrease rapidly within the bank of the sulcus where the anterior auditory field (AAF) is located (*Fleshman and Shamma 1988*; *Shamma et al. 1990*).

Representative maps of the distribution of the M values are shown in Figs. 11 and 12. In Fig. 11 we illustrate two maps with closely spaced electrode penetrations that were made orthogonally to the plane of the cortex and along isofrequency strips with BFs ranging from 1-10 kHz. Figure 12 summarizes experiments from 15 other animals. The value of M in any given penetration represents the averaged value of all tests performed in the penetration, which may include recordings of 2 or 3 separate units or unit clusters.

A consistent finding in our experiments is a clustering or a location dependent change in the values of the index M, due largely to a change in the efficacy of the inhibitory side-bands along the isofrequency contours. Specifically, at the center of AI, the response areas typically possess a narrow excitatory region often flanked by narrow and symmetric inhibitory side-bands and

M is near zero ($-0.07 < M < 0.07$; partially shaded circles in Figs. 11-12).

In most maps, moving caudally from the center of AI, the high frequency ($> BF$) inhibitory side-bands become broader and/or more potent than the low frequency side-bands ($< BF$). This is usually accompanied by a gradual broadening of the excitatory response area towards lower frequencies. The combined effect of these changes is to make the M values more negative ($M < -0.07$; clear circles in Figs. 11-12).

The opposite trends occur rostral to the center of AI. Low frequency inhibition is strengthened relative to the high frequency side-bands. This is sometimes accompanied by a spread of the $T1$ excitatory responses to higher frequencies, although not as commonly as the spread to low frequencies observed in the caudal penetrations. The combined effect of these trends is to increase the values of M ($M > 0.07$; filled circles in Figs. 11-12).

The distribution of the M values along the isofrequency planes spans all the frequencies tested (0.5–11 kHz) in an orderly manner to give the appearance of continuous bands that run orthogonal to the isofrequency contours (Fig. 10). In all maps, we have marked with dashed lines the borders of the region where M changes once from extreme positive to extreme negative values. These regions are quite variable in width. On average, they span about 1 mm along the surface of A1, but they may vary between 0.7-2 mm. Beyond the dashed lines, the responses may either become weak, or a reversal in M index values occurs (see for instance maps # 49, 65, 74, 102). In general, we did not investigate in detail the the number of repeated bands. This was partly due to experiment time limitations, and partly because the responses towards the edges of the AI often became weaker and units more difficult to isolate.

Topographic distribution of FM directional sensitivity

The correspondence established earlier between the response area type of a cell/cluster and its FM directional sensitivity suggests that FM sensitivity is also mapped in a regular fashion along the isofrequency planes of AI. This is confirmed in Fig. 13A where maps of the M and C indices were recorded from single-units in the same animal. Three additional FM maps are shown in Fig. 13B. In all these maps, the basic distribution pattern of the C index mirrors that already described for the M index earlier. In order to quantify the correspondence between the

response area type and FM maps, a scatter plot of the C versus M average penetration indices is compiled from all pairs of maps #'s 41, 43, 74, and 102 (Figs. 11, 12, and 13). The most significant feature in the plot is the clustering of the points along the diagonal, especially in the I and III quadrants. This, together with the positive slope of the regression line, indicate strong correlation between the indices of the penetrations in the two-tone and FM maps.

Topographic distribution of responses to spectrally shaped noise

The topographic distribution of the response area types can be further confirmed by a corresponding distribution of the S index computed from spectrally shaped noise stimuli. Figure 14 shows six such maps. Filled (clear) circles represent penetrations excited best by the noise band $\geq BF$ ($\leq BF$). These maps exhibit the same trends seen earlier with the two-tone stimulus in the corresponding maps in Figs. 11 and 12. Figure 14B illustrates the correspondence between the M and S average penetration indices in a scatter plot similar to that of Fig. 13C.

DISCUSSION

The data presented here suggest that there is an orderly change in the shape of response areas along the rostro-caudal isofrequency contours of the ferret primary auditory cortex. In the center of AI, responses are sharply tuned with symmetric and narrow inhibitory sidebands. Toward the edges of AI, the response areas become both broad and asymmetric, with high frequency ($> BF$) inhibition dominating caudally, and low frequency ($< BF$) inhibition dominating rostrally. These response area types form ordered repeating bands that traverse the isofrequency planes orthogonally. Superimposed on this map is an orderly change in the responses to FM tones along the isofrequency planes. Cells/Clusters with dominant inhibition from above (below) the BF respond selectively to upward (downward) frequency sweeps. At the center of AI, both directions are equally effective.

Interpreting multi-unit recordings

All cortical maps illustrated in this report (except for #102 in Fig. 13A) were constructed using a mix of single- and multi-unit records. In recording from clusters of cells, the trace may include action potentials from several cells of different types and sensitivities, as well as

thalamic afferents, all of which superimposed on a slow evoked potential. Furthermore, the occurrence of these spikes often overlap, and hence the number of events recorded may not always correspond to the actual total number of spikes occurring in the vicinity of the electrode tip. These problems place certain limitations on interpreting the results. Thus, one can at best say that the maps reflect ordered changes in neuronal activity integrated over small volumes in AI. Dissecting further the origins of such changes is difficult since the response of a cluster may in principle differ substantially from its underlying neurons. For instance, a broadly tuned cluster may be due to similarly tuned constituents, or to a collection of narrowly tuned cells at different BFs (*Schreiner and Mendelson 1990*).

All our recordings have been consistently obtained in the III and IV cortical layers, where single tones at BF evoke strong excitatory onset potentials. At these intermediate depths, and using tonal stimuli, single-unit and multi-unit records are quite similar (Fig. 7). These data are consistent with the observation that two response features – the BF and the symmetry of the response area – remain relatively stable in single-unit recordings over 400 μm of depth (Fig. 6), indicating a columnar organization of the response area type, and likely of other correlated features such as FM directional sensitivity.

Finally, it should be noted that the random character of the different sources of response variability (e.g., combining multi- and single-unit records, and the choice of stimulus parameters) can only serve to obscure regular trends in the maps. Consequently, evidence of systematic organization in the distribution of responses is a testimony to the robustness of its underlying causes.

Distribution of cortical response features

Gradual changes of monaural response properties along the isofrequency planes have been described previously, both in AI (*Schreiner and Mendelson 1990*; *Mendelson et al. 1988*; *Suga 1977*), in other cortical fields (*Schreiner and Urbas 1986*; *Schreiner and Urbas 1988*; *Serkov and Yanouskii 1971*), and in pre-cortical nuclei (*Rodrigues-Dagaeff et al. 1989*; *Schreiner and Langner 1988*). In AI, the maps of integrated excitation that Schreiner and Mendelson (1990) report in the cat are consistent with our response area maps. They show gradual broadening

of bandwidths away from the center, similar to the one sided spread of excitation seen in our asymmetric response areas. Interestingly, they also report a secondary narrowly tuned area which may correspond to the repeated nature of the response area map.

It is clear in our results that the balance of inhibitory inputs plays the critical role in shaping the symmetry of cortical response areas. The origin of this inhibition, however, is uncertain. The auditory cortex abounds with local inhibitory inter-neurons and inputs that may form the necessary substrate for these maps (*de Ribaupierre et al. 1972*; *Serkov and Yanouskii 1971*; *Serkov and Yanouskii 1974*). Furthermore, response areas with inhibition of different symmetries (as in Fig. 5) have recently been demonstrated in all cortical fields, and especially in AI, in the alert Monkey (*Schwarz and Tomlinson 1990*; *Shamma and Symmes 1985*). Lateral inhibition of various symmetries, however, also exists at all other auditory nuclei (*Aitken and Dunlop 1969*; *Martin and Dickson 1983*; *Moore et al. 1983*; *de Ribaupierre et al. 1972*; *Sachs et al. 1978*; *Suga 1965a*, 1969 Citecomma Voigt and Young 1980), as well as in other sensory systems (*Hartline 1974*; *Rall et al. 1966*). Consequently, it is uncertain whether the maps observed in these experiments are intrinsically cortical, or are manifestations of already formed maps at earlier centers (as is the case, for instance, for the binaural columns in the IC (*Wenstrup et al. 1986*)).

Several anatomical studies have hinted at extended intracortical connectivities along the isofrequency planes (e.g. Matsubara and Phillips 1988; Wallace et al. 1991). Specifically, Matsubara and Phillips (1988) showed that microinjections of tracer in a group of AI neurons that are homogeneous with respect to their BF's and binaural response properties, labeled as many as five patches of cells roughly spaced at 0.8-1.5 mm along the isofrequency planes. Since the labeled regions were heterogeneous with respect to their binaural responses, they hypothesized that these connectivities may help fine-tune such monaural response properties as "side-band inhibition or sensitivity to frequency-modulated sound signals". This conjecture is supported by our physiological mappings. Furthermore, it is quite plausible that the patchy appearance of the anatomically labeled regions underlies the repeated character of the physiological maps.

Finally, there are indirect correspondences between our maps and those representing the

amplitude-spectrum in the DSCF area of the AI in the mustached bat (Suga and Manabe 1982). In the latter, side-band inhibition creates an "amplitopic representation" of the important 62 kHz component of the bat's biosonar signal, using cells tuned to different "best amplitudes" and arranged in an orderly fashion. While in ferret AI the inhibitory response areas take various asymmetric forms around the central excitatory area, it is most probably the *strength* of the inhibition, and not its *asymmetry* per se, that is responsible for nonmonoticity in cortical cells, and hence their "amplitude tuning". Since we did not quantify specifically the strength of the inhibition nor the nonmonoticity of the responses in our maps, it is difficult to say whether the asymmetry index is related to a gradient of inhibition or nonmonoticity along the isofrequency planes. However, Schreiner and Mendelson (1990) found systematic spatial distribution of step-response magnitudes in the cat which they argued reflects inhibition strength.

Functional interpretation of response area maps: Spectral gradient columns

From a functional point of view, there are two possible implications to this organization of the response areas. The first is that the response areas are directly responsible for the FM sensitivity and its ordered mapping along the isofrequency planes. Recent preliminary mappings in the cat's AI have exhibited similar, but not identical, FM maps (*Mendelson et al. 1988*). The correspondence between the response areas' asymmetry and the direction of FM sensitivity has previously been demonstrated in the bat auditory system (*Suga 1965a*, 1965b, 1969). A direct analogue of this phenomenon may exist in the visual system where motion direction and edge orientation sensitivity are strongly correlated in the responses of the primary visual cortex (*Hubel and Wiesel 1962*, 1968; *Marr 1982*).

This leads to the second interpretation of the results, namely that the response area maps primarily function to generate an explicit representation of the acoustic spectrum along the isofrequency planes. This is because a change in the symmetry of response areas along a particular isofrequency plane causes cells along this axis to respond differentially reflecting the distribution of spectral energy around their BF, i.e., the local spectral shape. For instance, relatively narrow and symmetric spectral peaks (e.g., those due to low intensity single tones or a sharp resonance in a complex spectrum) excite best cells near the center of the corresponding

isofrequency planes where thresholds are lowest and little or no inhibition is recruited from the side-bands. However, for skewed spectral peaks or spectral edges, the locus of the maximal response shifts away from the center of the isofrequency plane towards cells with response areas of the opposite asymmetry, such that the input recruits the least inhibition. Consequently, in relation to the ferret maps (e.g. Fig. 11), broadening of an input spectral peak towards higher frequencies causes a rostral shift in the maximal cortical response, since cells in caudal regions are more strongly inhibited above BF. The opposite shift occurs if the input peak is oriented towards lower frequencies.

Therefore, the organization of the response areas suggests a model in which the shape of the spectral envelope is encoded explicitly in the two-dimensional distribution of neural activity across the extent of AI. A concise statement of the model is that *the location of the maximal response along a particular isofrequency plane encodes the locally smoothed gradient of the spectrum at that frequency.* This mapping scheme provides a neurophysiological basis for the significant role that spectral gradients play in timbre perception and the recognition of complex sounds (*Plomp 1976*). For instance, experiments on the perceptual distances between phonetic categories have revealed that the distance metrics that best correlate with perception are those based on spectral gradients, rather than on the spectrum itself (*Assmann and Summerfield 1989*; *Klatt 1982*). Furthermore, human subjects exhibit consistently high sensitivities to direct perceptual correlates of these physiological maps, namely to changes in spectral peak symmetry (*Shamma et al. 1992*).

Relation to spatial frequency selectivity and orientation columns in the visual cortex

The functional interpretation of the response area maps as *spectral gradient* maps has close parallels in the visual cortex. There, receptive fields (in two-dimensional form) of various asymmetries are common, and are thought to be involved in the production of ordered maps of spatial frequency selective channels and orientation sensitivity (*de Valois and de Valois 1988*; *Jones and Palmer 1987*). This suggests a common organizational principle that unifies the primary auditory and visual cortical representations: *Both encode the locally smoothed gradients of their input patterns.* For the one-dimensional world of auditory inputs, this encoding principle

translates to sensitivity to the phase of the spectral envelopes, and hence to peak symmetries and spectral tilts. For the two-dimensional world of visual images, it translates to sensitivity to spatial phase and edge orientations, which are specified by spatial gradients in two directions (de Valois and de Valois 1988). This hypothesis can presumably be readily tested with anatomical mappings (e.g., 2-DG technique or cyt-ox staining) analogous to those used to establish the orientation and spatial frequency organization in primary visual cortex (de Valois and de Valois 1988). For instance, "gradient specific slabs" may emerge when using acoustic stimuli with opposite spectral asymmetries and that span all frequencies, such as the noise stimuli used in our experiments.

Finally, the above hypotheses are in harmony with recent experimental results in which retinal cells of newborn ferrets were induced to project to the auditory thalamus and cortex (*Sur et al. 1988*). Many cortical cells in the adult animal then exhibited visually driven responses, with oriented receptive fields and other features typical of the visual cortex. A possible implication of these findings and of the auditory maps presented here is that the development of primary auditory and visual cortical maps may diverge largely because of the different nature of their inputs, rather than of their underlying functional principles.

Acknowledgement

This work is supported in part by grants from the Air Force Office of Scientific Research, Office of Naval Research, and the Naval Research Laboratory. We would like to thank J. Virdy and P. Gopalaswamy for their help in developing the data acquisition system, and A. Owens and N. Kowalski for their assistance in data recordings. We are also grateful to Drs. N. Suga, C. Carr, and anonymous reviewers for their detailed and critical comments on the original manuscript. The authors are members of the Systems Research Center which is partially funded by an NSF grant (# NSFD CD 8803012).

REFERENCES

Abeles, M. and Goldstein, M.H. Functional architecture in cat primary auditory cortex: columnar organization and organization according to depth. *J. Neurophysiol.* 33: 172-187, 1972.

Aitken, L.M. and Dunlop, C.W. Inhibition in the medial geniculate body of the cat. *Exp. Brain Res.* 7: 68-83, 1969.

Assmann, P.F. and Summerfield, Q. Modelling the perception of concurrent vowels: Vowels with the same fundamental frequency. *J. Acoust. Soc. Am.* 85: 327-338, 1989.

Brugge, J.F., Dubrovsky, N.A., Aitken, L.M., and Anderson, D.J. Sensitivity of single neurons in auditory cortex of cat to binaural tonal simulation: Effects of varying interaural time and intensity. *J. Neurophysiol.* 32: 1005-1024, 1969.

Brugge, J.F. and Merzenich, M.M. Responses of neurons in auditory cortex of the Macaque monkey to monaural and binaural stimulation. *J. Neurophysiol.* 36: 1138-1158, 1973.

Evans, E.F. Single-unit studies of mammalian cochlear nerve. In: *Auditory investigation: The scientific and technological basis*, edited by H.A. Beagley. Oxford: Clarendon Press, 324-367, 1979.

Evans, E.F. and Whitfield, I.C. Classification of unit response in the auditory cortex of the unanaesthetized and unrestrained cat. *J. Physiol. (London)* 171: 476-493, 1964.

Fleshman, J.W. and Shamma, S.A. Organization of the ferret auditory cortex. *Acoust. Soc. Am. Abstr.* S1 84: 56, 1988.

Hartline, H.K. Studies on excitation and inhibition in the retina. New York: Rockefeller University Press, 1984.

Hubel, D.H. and Wiesel, T.N. Receptive fields, binocular interaction and functional architecture in the cat's visual cortex. *J. Physiol. (London)* 160: 106-154, 1962.

Hubel, D.H. and Wiesel, T.N. Receptive fields and functional architecture of monkey striate cortex. *J. Physiol. (London)* 195: 215-243, 1968.

Imig, T.J. and Adrian, H.O. Binaural columns in the primary field (AI) of cat auditory cortex. *Brain Res.* 138: 241-257, 1977.

Jenkins, W.M. and Merzenich, M.M. Role of cat primary auditory cortex for sound- localization behavior. *J. Neurophysiol.* 52: 819-847, 1984.

Jones, J.P. and Palmer, L.A. The two-dimensional spatial structure of simple receptive fields in cat striate cortex. *J. Neurophysiol.* 58: 1187-1211, 1987.

Kavanagh, G.L. and Kelly, J.B. Contribution of auditory cortex to sound localization by ferret *Mustela putorius*. *J. Neurophysiol.* 57: 1746-1766, 1987.

Kelly, J.B., Judge, P.W., and Phillips, D.P. Representation of the cochlea in primary auditory cortex of the ferret *Mustela putorius*. *Hearing Res.* 24: 111-115, 1986.

Klatt, D.H. Prediction of perceived phonetic distance from critical-band spectra: A first step. *Proc. ICASSP* 82: 1278, 1982.

Marr, D. *Vision.* New York: Freeman and Company, 1982.

Martin, M.P. and Dickson, J. Lateral inhibition in the anteroventral cochlear nucleus of the cat: A microiontophoretic study. *Hearing Res.* 9: 35-41, 1983.

Matsubara, J.A. and Phillips, D.P. Intracortical connections and their physiological correlates in the primary auditory cortex (AI) of the cat. *J. Comp. Neurol.* 268: 38-48, 1988.

Mendelson, J.R., Schreiner, C.E., Grasse, K.L., and Sutter, M.L. Spatial distibution of responses to FM sweeps in cat primary auditory cortex. *A.R.O. meeting* 11: abstr. 240, 1988.

Merzenich, M.M., Knight, P.L., and Roth, G.L. Representation of cochlea within primary auditory cortex in the cat. *J. Neurophysiol.* 28: 231-249, 1975.

Merzenich, M.M., Kaas J.H., and Roth, G.L. Auditory cortex in the grey squirrel: tonotopic organization and architectonic fields. *J. Comp. Neurol.* 166: 387-402, 1976.

Middlebrooks, J.C., Dykes, R.W., and Merzenich, M.M. Binaural response-specific bands in primary auditory cortex (AI) of the cat: Topographical organization orthogonal to isofrequency contours. *Brain Res.* 181: 31-48, 1980.

Moore, D.R., Semple M.N., and Addison, P.D. Some acoustic properties of neurons in the ferret inferior colliculus, *Brain Res.* 269: 69-82, 1983.

Neff, W.D., Diamond, I.T., and Casseday, J.H. Behavioral studies of auditory discrimination: Central nervous system. In: *Handbook of Sensory Physiology*, edited by W.D. Keidel and W.D. Neff. Berlin: Springer-Verlag, 1975, p. 307-400.

Pfingst, B.E., and O'Connor, T.A. Characteristics of neurons in auditory cortex of monkeys performing a simple auditory task. *J. Neurophysiol* 45: 16-34, 1981.

Phillips, E.P., Ormand, S.S., Musicant, A.D., and Wilson, G.F. Neurons in the cat's primary auditory cortex distinguished by their responses to tones and wide-spectrum noise. *Hearing Res.* 18: 73-86, 1985.

Plomp, R. In: *Aspects of Tone Sensation.* Academic Press, 1976.

Rall, W., Shepherd G.M., Reese, T.S., and Brightman, M.W. Dendro-dendritic synaptic pathway for inhibition in the olfactory bulb. *Exp. Neurol.* 14: 44-56, 1966.

Reale, R.A. and Imig, T.J. Tonotopic organization of auditory cortex in the cat. *J. Comp. Neurol.* 192: 265-291, 1980.

de Ribaupierre, F., Goldstein M.H., and Yani-komshian, G. Intracellular study of the cat's primary auditory cortex. *Brain Research* 48: 185-204, 1972.

Rodrigues-Dagaeff, C., Simm, G., de Ribaupierre, Y., Villa, A., de Ribaupierre, F., and Rouiller, E. Functional organization of the ventral division of the medial geniculate body of the cat: Evidence for a rostro-caudal gradient of response properties and cortical projections. *Hearing Res.* 38: 103-126, 1989.

Sachs, M.B., Sinnott, J.M., and Heinz, R. Behavioral and physiological studies of hearing in birds. *Fed. Proc.* 37: 2329-2335, 1978.

Schreiner, C.E. and Langner, G. Periodicity coding in the inferior colliculus of the cat. II. Topographical organization. *J. Neurophysiol.* 60: 1823-1840, 1988.

Schreiner, C.E. and Mendelson, J.R. Functional topography of cat primary auditory cortex: Distribution of integrated excitation. *J. Neurophysiol.* 64: 1442-1459, 1990.

Schreiner, C.E. and Urbas J.V. Representation of amplitude modulation in the auditory cortex of the cat. I. Anterior auditory field. *Hearing Res.* 21: 227-241, 1986.

Schreiner, C.E. and Urbas, J.V. Representation of amplitude modulation in the auditory cortex of the cat. II. Comparison between fields. *Hearing Res.* 32: 49-64, 1988.

Schwarz, D.W. and Tomlinson, R.W. Spectral response patterns of auditory cortical neurons to harmonic complex tones in alert monkey (Macaca mulatta). *J. Neurophysiol.* 64: 282-297, 1990.

Serkov, F. and Yanouskii, E. Postsynaptic potentials of neurons of the cat auditory cortex. *Neurofiziologiya* 3: 339-349, 1971.

Serkov, F. and Yanouskii, E. Characteristics of cortical inhibitory neurons. *Neurofiziologiya* 6: 119-126, 1974.

Shamma S.A., Fleshman, J.W., and Wiser, P.R. Receptive field organization in primary auditory cortex. *Tech. Rep. Systems Research Center, Univ. of Md.* TR 90: 46, 1990.

Shamma, S.A., Vranic, S., and Wiser, P.R. Spectral gradient columns in primary auditory cortex: Physiological and Psychoacoustical correlates. In: *Auditory physiology and perception, Advances in the Biosciences Vol. 83*, edited by Y. Cazals, L. Demany, and K. Horner. Oxford: Pergamon Press, 1992, p. 397-406.

Shamma, S.A. and Symmes, D. Patterns of inhibition in auditory cortical cells in awake squirrel monkeys. *Hearing Res.* 19: 1-13, 1985.

Suga, N. Analysis of frequency-modulated sounds by auditory neurons of echo locating bats. *J. Physiol. (London)* 179: 26-53, 1965a.

Suga, N. Functional properties of auditory neurons in the cortex of echolocating bats. *J. Physiol. (London)* 181: 671-700, 1965b.

Suga, N. Classification of inferior collicular neurons of bats in terms of responses to pure tone, FM sounds, and noise bursts. *J. Physiol. (London)* 200: 555-574, 1969.

Suga, N. Amplitude spectrum representation in the Doppler-shifted-CF processing area of the auditory cortex of the mustache bat. *Science* 196: 64-67, 1977.

Suga, N. The extent to which biosonar information is presented in the bat auditory cortex. In: *Dynamic Aspects of Neocortical function*, edited by G.M. Edelman, W.E. Gall, and W.M. Cowan. New York: Wiley, 1984, 315-337.

Suga, N. and Manabe, T. Neural basis of amplitude-spectrum representation in the auditory cortex of the mustached bat. *J. Neurophysiol.* 47: 225-255, 1982.

Suga, N. and O'Neill, W.E. Neural axis representing target range in the auditory cortex of the mustached bat. *Science* 206: 351-353, 1979.

Sur, M., Garraghty, P.E., and Roe, A.W. Experimentally induced visual projections into auditory thalamus and cortex. *Science* 242: 1437-1441, 1988.

de Valois, R.L. and de Valois, K.K. *Spatial vision.* New York: Oxford University Press, 1988.

Voigt, H.F. and Young, E.D. Evidence of inhibitory interactions between neurons in the dorsal cochlear nucleus. *J. Neurophysiol.* 44: 76-96, 1980.

Wallace, M.N., Kitzes, L.M., and Jones, E.G. Intrinsic inter- and intralaminar connections and their relationship to the tonotopic map in cat primary auditory cortex. *Exp. Brain Res.* 86: 527-544, 1991.

Wenstrup, J.J., Ross, L.S., and Pollak, G.D. Binaural response organization within a frequency band representation of the inferior colliculus: implications for sound localization. *J. Neurosci.* 6: 962-973, 1986.

Whitfield, I.C. Auditory cortex and the pitch of complex tones. *J. Acoust. Soc. Am.* 67: 644-647, 1980.

Zeki, S. and Shipp, S. The functional logic of cortical connections. *Nature* 335: 311-317, 1988.

Figure Legends

Figure 1

Measuring the range of the inhibitory and excitatory responses using a two-tone stimulus.

A: Rasters illustrating the responses of a multi-unit cluster to each of the two tones separately (top two rasters), and to the combined tones (bottom raster).

Top raster illustrates the responses to the conditioning tone, $T1$, which is presented at 100 ms into the sweep, for a duration of 200 ms. $T1$ Tone intensity is 65 dB SPL; its frequency spans ± 1 octaves around the BF(=8 kHz) in 1/4 octave steps (labeled only every other step). $T1$ responses start approximately 16 ms following the onset of the tone (i.e., at 116 ms). They are usually restricted to a limited range of frequencies around the BF which defines the excitatory response area of the cell at that $T1$ intensity. Please note that here, as in all other rasters in this paper, the frequencies are rounded and labeled only to one or two significant places after the decimal. In reality, however, frequencies were determined and presented at better than 99.999% accuracy. Ten repetitions are made at each $T1$ frequency.

Middle raster illustrates the responses to the second (test) tone, $T2$, alone. $T2$ onset is usually delayed relative to onset of $T1$ (by 25 ms in this case) and lasts for 200 ms. Its frequency is fixed throughout the test at the BF of the cell. $T2$ intensity here is 60 dB SPL.

Bottom raster (two-tone raster) illustrates the responses to the two tones presented simultaneously. Frequency of the $T1$ burst is indicated on the left. Ten repetitions of the stimulus are made at each $T1$ frequency. The phasic responses of the cell to the two tones are segregated because of the inter-tone delay. $T2$ responses start at 144 ms. They are vigorous when $T1$ is not near BF and are reduced otherwise. The inhibitory response area is defined by the range of $T1$ frequencies and intensities which reduces $T2$ responses. The bold arrows along the time axis represent the interval over which the responses to the two tones are counted.

B: Response amplitude as a function of $T1$ frequency. The solid curve represents the excitatory onset response of $T1$ counted over the 35 ms window (100–135 ms) indicated by the bold arrows along the time axis of the top raster in **A** above. Dashed curve is the response to the onset of $T2$ counted over the 45 ms window (136–180 ms) marked by the bold arrows in

the middle raster of **A**.

C: The total response amplitude as a function of $T1$ frequency. Events are counted over the 80 ms long window (100–180 ms) marked by the bold arrows in the two-tone raster in **A**, i.e., it is the sum of the solid and dashed response curves in the plot above.

Figure 2

Typical raster responses of cell clusters with three different patterns of inhibition: symmetric side-band inhibition (figures in column **I**), and asymmetric inhibition (columns **II** and **III**).

A: Rasters of responses to the two-tone stimulus. Lateral inhibition is evidenced by the near absence of responses to either tone. Such frequency regions are marked by the side arrows.

B: Response amplitude as a function of $T1$ frequency. The solid and dashed curves in each plot are as in Fig. 1B.

C: The total response amplitude as a function of $T1$ frequency. For each curve, events are counted over the 80 ms long window (100–180 ms) marked by the bold arrows in the raster above it.

All raster displays in this paper are labeled on top by a code used to identify each test record (e.g., the label $065/34a01.t2$ in Fig. 2A).

Figure 3

Examples of the variability of responses for the three types of inhibition: symmetric inhibition (**A**), above BF inhibition (**B**), and below BF inhibition (**C**). In all rasters, $T1$ frequencies span $\pm$ 1 or $\pm$ 2 octaves around the BF, at 1/8 or 1/4 octave resolution; $T1$ intensity is indicated to the right of each raster. The plot in the right inset figure of each raster is of the total response amplitude curve computed from the time window 100-180 ms, i.e., exactly as in Figs. 1C and 2C except plotted sideways against the same frequency axis of the raster. The value of the index M computed from this plot is shown in the bottom left corner of each raster.

Figure 4

Stability of two-tone responses with respect to changes in inter-tone delays. *top row* inter-tone delays (from left to right): 25,12.5,0 ms. *Bottom row* inter-tone delays: 50,12.5,0 ms.

Figure 5

Three response area types of single units in AI.

A: A response area with weak symmetric inhibition. The borders of the inhibitory response areas (shaded) and the excitatory response areas (white) are deduced from two-tone response amplitude curves similar to those in Fig. 1B. The two axes indicate the intensity and frequency of $T1$. The intensity and frequency of $T2$ are indicated by the "**X**" in the figure.

B: A response area with asymmetric inhibition below the BF.

C: A response area with asymmetric inhibition above the BF.

Figure 6

A: Columnar organization of response area types of cells in the intermediate layers of the primary auditory cortex. Shown are response areas of cells at various depths from three separate penetrations (**I, II, III**). The inhibitory (shaded) and the excitatory (white) response areas are computed as in Fig. 5. In penetration **I**, the response areas exhibit strong inhibition above the BF. In **II** the response areas are more symmetric. In **III** the response areas have broad inhibition below the BF. Note that all cells in this penetration are strongly nonmonotonic as indicated by the inhibitory responses in the center of the excitatory area.

B: Consistency of M index values within a column. Left distribution is for the index M values computed from the response areas of 66 cortical cells (16 penetrations in 5 animals). Right distribution is of the deviation of each of the above M indices from the average index value of all single-units within its column. Index values outside of the range ± 0.07 reflect either asymmetric response areas (left panel) or large deviations from the penetration mean (right panel).

Figure 7

A: Two examples of the correspondence between responses from a cluster of cells and its constituent single units. In each row, the left raster is the response of a cluster (2-4 cells). The responses of a single unit from the cluster are shown to the right. Note the consistent pattern of inhibition in each case as indicated by the M asymmetry index.

B: M index values derived from single-unit recordings versus M values from multi-unit cluster responses recorded at the same location in the cortex. Clustering along the diagonal,

especially in the I and III quadrants, indicates good correspondence between the two indices. The solid line represents the linear regression: $M_{unit} = 1.28M_{cluster} - 0.02$, $r = 0.47$, N = 61. The correlation is significant ($P < 0.001$, t test).

Figure 8

A Correspondence between responses to two-tone (top row of rasters) and FM stimuli (bottom row). The parameters of the FM stimulus are illustrated below the middle rasters for two different sweep rates. Tones were swept either linearly or at an exponentially increasing rate, i.e., keeping a constant rate along the approximately logarithmic tonotopic axis. Both types of sweeps produce essentially similar responses. The trajectory of the frequency values in each 500 ms trial is shown below the figure. The frequency is first swept upwards from an octave below BF to an octave above it; it is maintained at $2BF$ for a short period, and then swept downwards in the opposite direction. For all rates (indicated by the numbers to the left of the raster), the stimulus is designed such that the BF is always traversed at the same times into the trial (at 100 ms for the upward sweep, and at 400 ms for the downward sweep). The responses to the up and down sweeps, $R\uparrow$ and $R\downarrow$, are measured in the 100-150 ms and 375-425 ms time windows, respectively. These intervals are indicated by the bold arrows in the rasters. The intensity of the FM tone is indicated to the right of the raster. In the left column of rasters, the response is strongly inhibited from below the BF, and is selectively sensitive to downward sweeps. The opposite case is shown in the right column. The middle response is relatively symmetric.

B: Correspondence between the asymmetry index M and the FM directional sensitivity index C. Data are obtained from 46 multi-unit clusters in 5 ferrets. For M the average of indices at 65 and 75 dB SPL is computed; C is derived from FM tests at 70 dB SPL. The solid line represents the linear regression: $C = 1.00M - 0.06$, $r = 0.49$, N = 46. The correlation is significant ($P < 0.001$, t test).

Figure 9

Correspondence between responses to two-tone (top row of rasters) and spectrally shaped noise (bottom row) stimuli in three different types of response areas. Schematic spectra of the

three noise stimuli used to measure the symmetry of the response areas are shown to the left of the bottom rasters. All responses are measured in the 100-150 ms time window indicated by the bold arrows. The numbers to the left of the bottom rasters indicate the left/right slopes of the noise spectrum around the BF. The index C values for the three cells are (from left to right): 0.14, 0.03, -0.13.

Figure 10

Approximate location of the primary auditory cortex (AI) in the ferret cortex. Schematic below shows a magnified view of the tonotopic organization and borders of AI relative to the supra-sylvian fissure and the physiologically defined anterior auditory field (AAF). The numbers indicate the $BF's$ measured at the penetrations marked by the dots. Approximate iso-frequency planes are represented by the rostro-caudally oriented lines. The (M)edial and (R)ostral directions are indicated by the arrows; Arrow lengths represent 1 mm distances on the surface of the cortex.

Figure 11

The distribution of the *two-tone* response symmetry measure, M, in the ferret primary auditory cortex from two animals (# 65 and #74). The circles indicate the locations of the electrode penetrations along the isofrequency contours (shown schematically as solid straight lines); asterisks mark penetrations with weak auditory responses. The arc in each map represents the location of the supra-sylvian fissure; the dashed lines delineate the approximate borders of the band within which the M measure changes from extreme negative (clear circles) to extreme positive values (filled circles). A key for the classification scheme used is shown on the left of the figure. The (M)edial and (R)ostral directions are indicated by the arrows; the arrow lengths represent 1/2 mm distances on the surface of the cortex.

Figure 12

Maps of the distribution of M values in the AI of 15 additional ferrets. Details are as in Fig. 11 map.

Figure 13

A: Comparison of the topographic distribution of two-tone and FM responses in AI. Map on the left is of the index M derived as in Fig. 11. Map on the right shows the corresponding distribution of the C index computed from FM responses of the same cells as in the left map. Map features and symbols are as in Fig. 11. Filled (clear) circles mark penetrations with selective responses to downward (upward) sweeps. Partially shaded penetrations are less selective.

B: Three further examples of the distribution of FM directional sensitivity. The corresponding maps of response area symmetry are found in Figs. 11, and 12.

C: Scatter plot of the average C versus the average M indices for all penetrations shown in maps of Figs. 13A and B. The plot compares the (classified) index values of each penetration using the two stimuli. To facilitate the comparison, an arbitrary uniform numerical scale is assigned to the different classes ranging from -1 (clear circles) to 1 (filled circles). The number of penetrations at each point of the plot is also indicated. The solid line represents the linear regression: $C = 0.75M - 0.15$, $r = 0.50$, N = 82. The correlation is significant ($P < 0.001$).

Figure 14

A: Maps of the distribution of S values in AI using spectrally shaped noise stimuli. All map features are similar to those of Fig. 11. The 6 maps are from animals also tested with two-tone stimuli and whose maps are shown in Figs. 11 and 12.

B: Scatter plot of the average S versus the average M indices for all penetrations shown in maps of Fig. 14B. The plot compares the (classified) index values of each penetration using the two stimuli. Details are as in Fig. 13C. The solid line represents the linear regression: $S = 0.53M - 0.08$, $r = 0.58$, N = 101. The correlation is significant ($P < 0.001$).

A

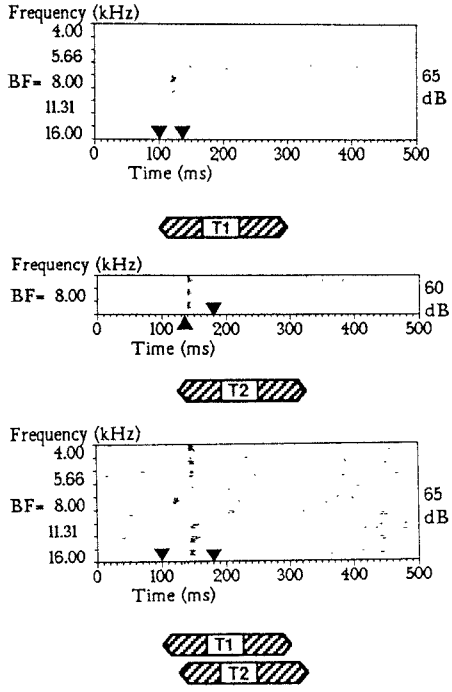
Frequency (kHz)
4.00
5.66
BF= 8.00
11.31
16.00
65
dB
0
100
200
300
400
500
Time (ms)
T1
Frequency (kHz)
BF= 8.00
60
dB
0
100
200
300
400
500
Time (ms)
T2
Frequency (kHz)
4.00
5.66
BF= 8.00
11.31
16.00
65
dB
0
100
200
300
400
500
Time (ms)
T1
T2

B

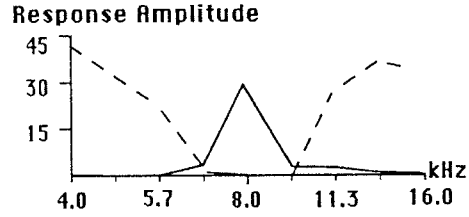
Response Amplitude
45
30
15
kHz
4.0
5.7
8.0
11.3
16.0

C

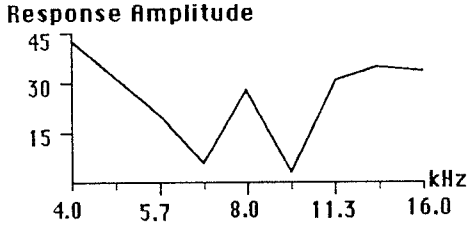
Response Amplitude
45
30
15
kHz
4.0
5.7
8.0
11.3
16.0

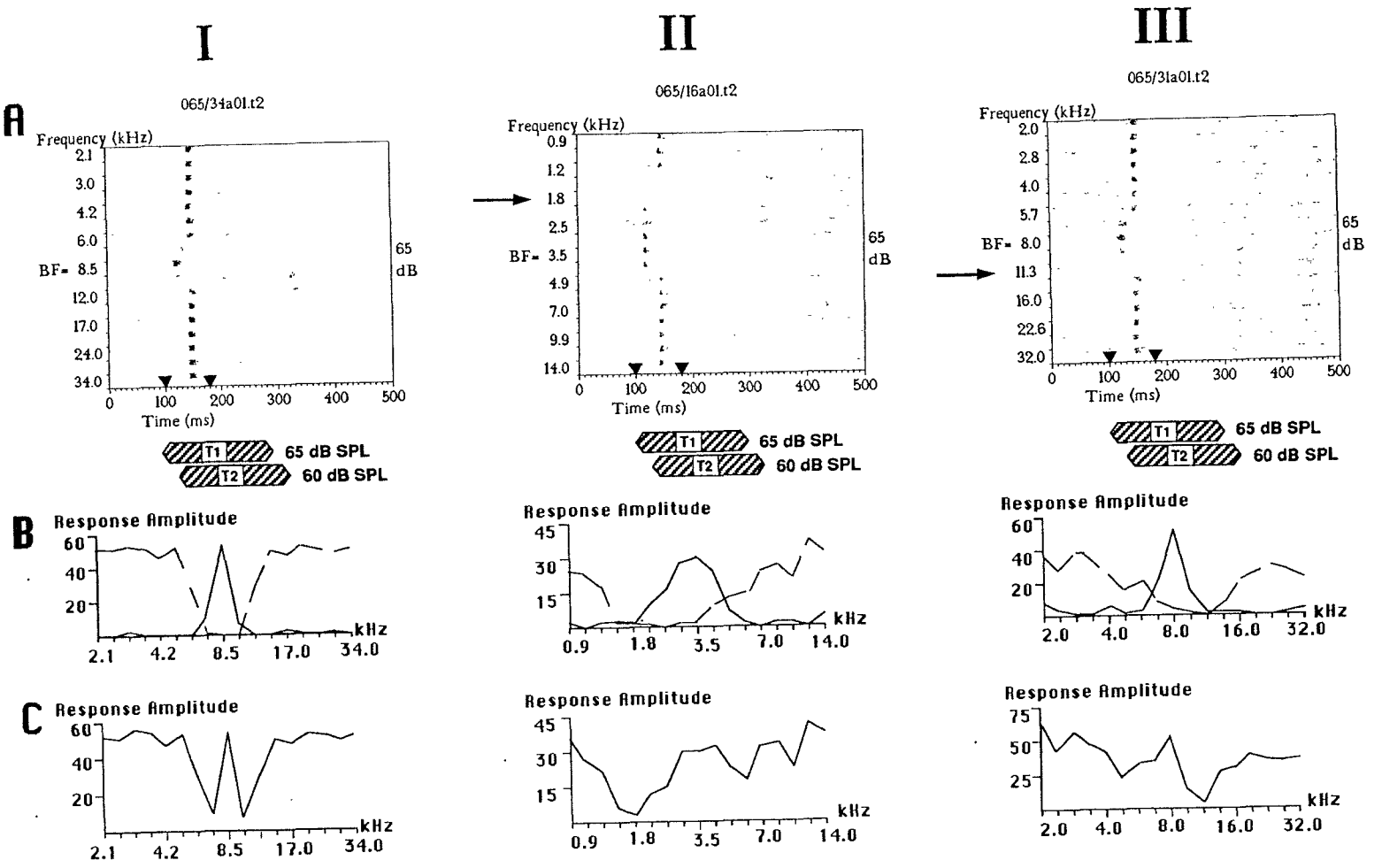
I
II
III
A
B
C
065/34a01.t2
065/16a01.t2
065/31a01.t2
Frequency (kHz)
2.1
3.0
4.2
6.0
BF= 8.5
12.0
17.0
24.0
34.0
0.9
1.2
1.8
2.5
BF= 3.5
4.9
7.0
9.9
14.0
2.0
2.8
4.0
5.7
BF= 8.0
11.3
16.0
22.6
32.0
65 dB
0
100
200
300
400
500
Time (ms)
T1
T2
65 dB SPL
60 dB SPL
Response Amplitude
kHz
2.1
4.2
8.5
17.0
34.0
0.9
1.8
3.5
7.0
14.0
2.0
4.0
8.0
16.0
32.0

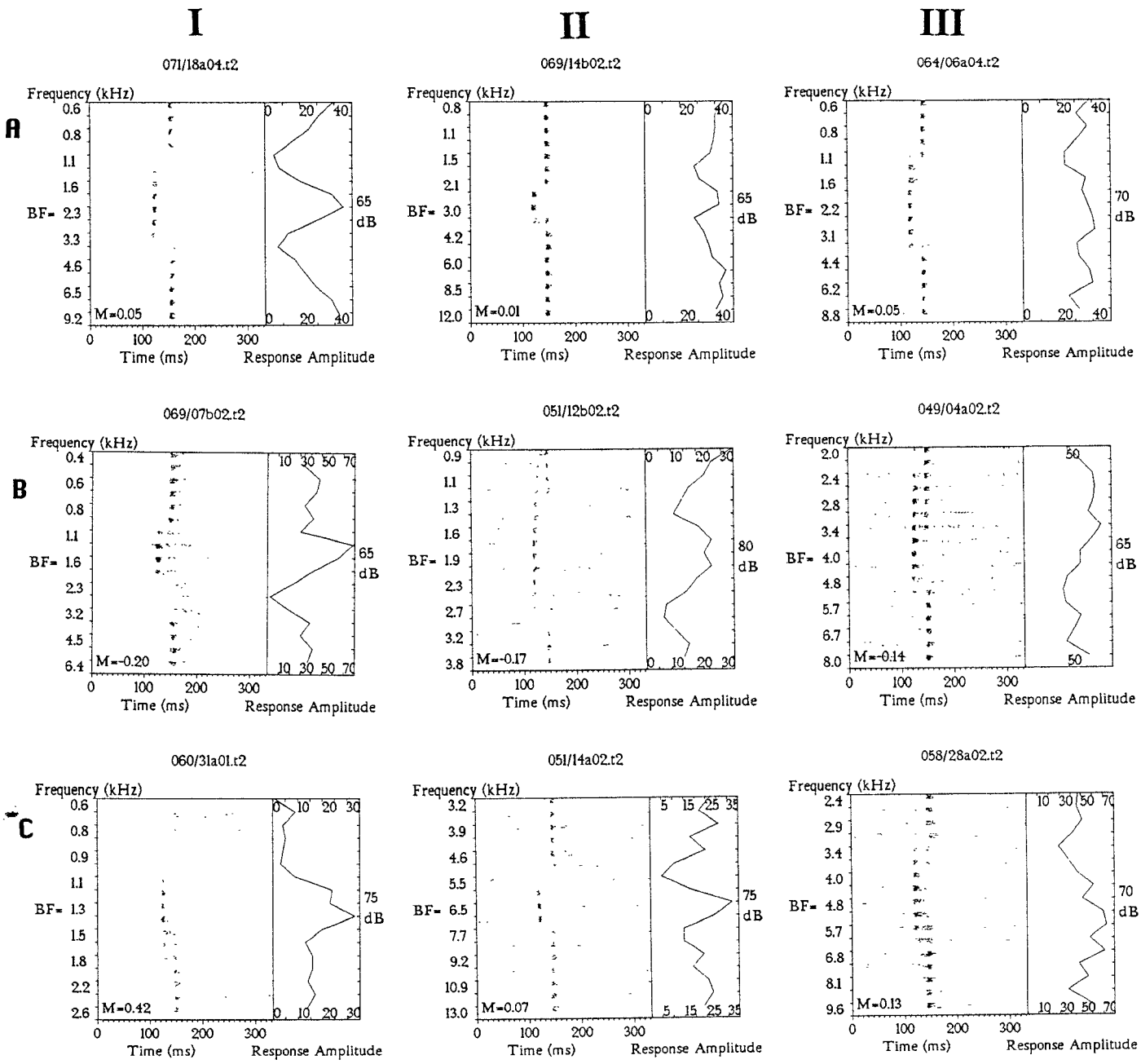
I
II
III
071/18a04.t2
069/14b02.t2
064/06a04.t2
A
Frequency (kHz)
BF= 2.3
M=0.05
65 dB
BF= 3.0
M=0.01
65 dB
BF= 2.2
M=0.05
70 dB
Time (ms)
Response Amplitude
069/07b02.t2
051/12b02.t2
049/04a02.t2
B
BF= 1.6
M=-0.20
65 dB
BF= 1.9
M=-0.17
80 dB
BF= 4.0
M=-0.14
65 dB
060/31a01.t2
051/14a02.t2
058/28a02.t2
C
BF= 1.3
M=0.42
75 dB
BF= 6.5
M=0.07
75 dB
BF= 4.8
M=0.13
70 dB

Fig 3

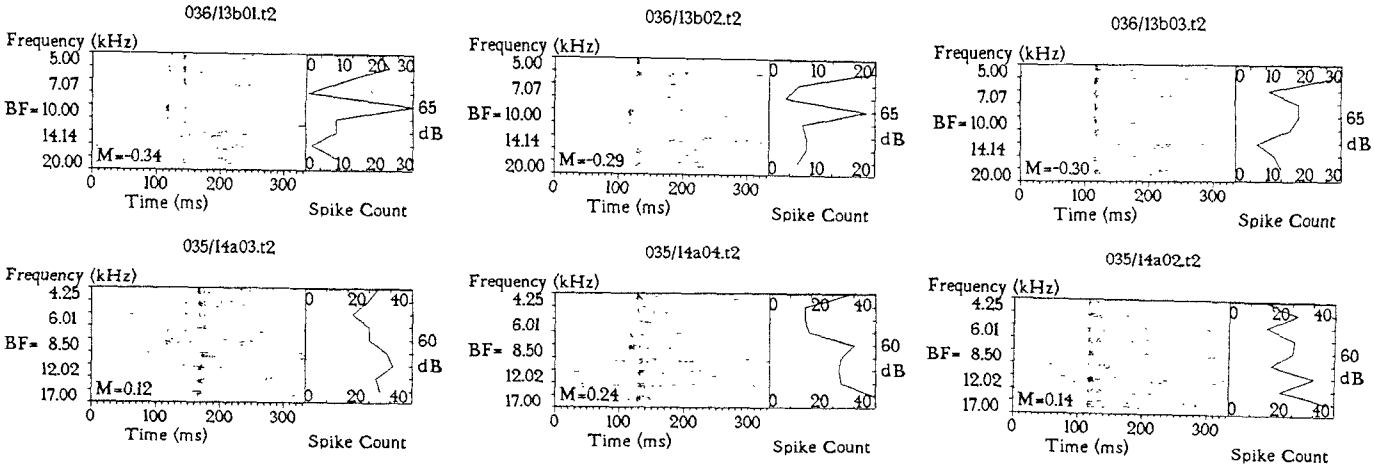
036/13b01.t2
Frequency (kHz)
5.00
7.07
BF= 10.00
14.14
20.00
M=-0.34
0 100 200 300
Time (ms)
0 10 20 30
0 10 20 30
65
dB
Spike Count
036/13b02.t2
Frequency (kHz)
5.00
7.07
BF= 10.00
14.14
20.00
M=-0.29
0 100 200 300
Time (ms)
0 10 20
0 10 20
65
dB
Spike Count
036/13b03.t2
Frequency (kHz)
5.00
7.07
BF= 10.00
14.14
20.00
M=-0.30
0 100 200 300
Time (ms)
0 10 20 30
0 10 20 30
65
dB
Spike Count
035/14a03.t2
Frequency (kHz)
4.25
6.01
BF= 8.50
12.02
17.00
M=0.12
0 100 200 300
Time (ms)
0 20 40
0 20 40
60
dB
Spike Count
035/14a04.t2
Frequency (kHz)
4.25
6.01
BF= 8.50
12.02
17.00
M=0.24
0 100 200 300
Time (ms)
0 20 40
0 20 40
60
dB
Spike Count
035/14a02.t2
Frequency (kHz)
4.25
6.01
BF= 8.50
12.02
17.00
M=0.14
0 100 200 300
Time (ms)
0 20 40
0 20 40
60
dB
Spike Count

Fig 4

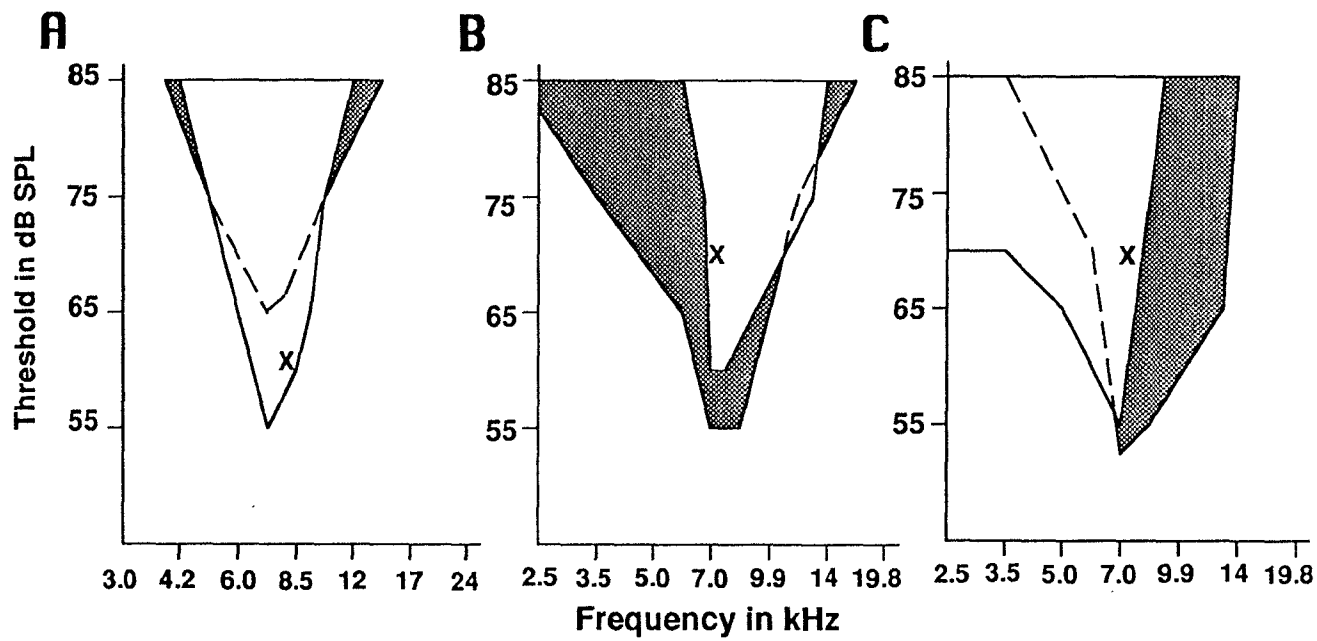
A
B
C
85
75
65
55
Threshold in dB SPL
X
3.0 4.2 6.0 8.5 12 17 24
2.5 3.5 5.0 7.0 9.9 14 19.8
Frequency in kHz

5

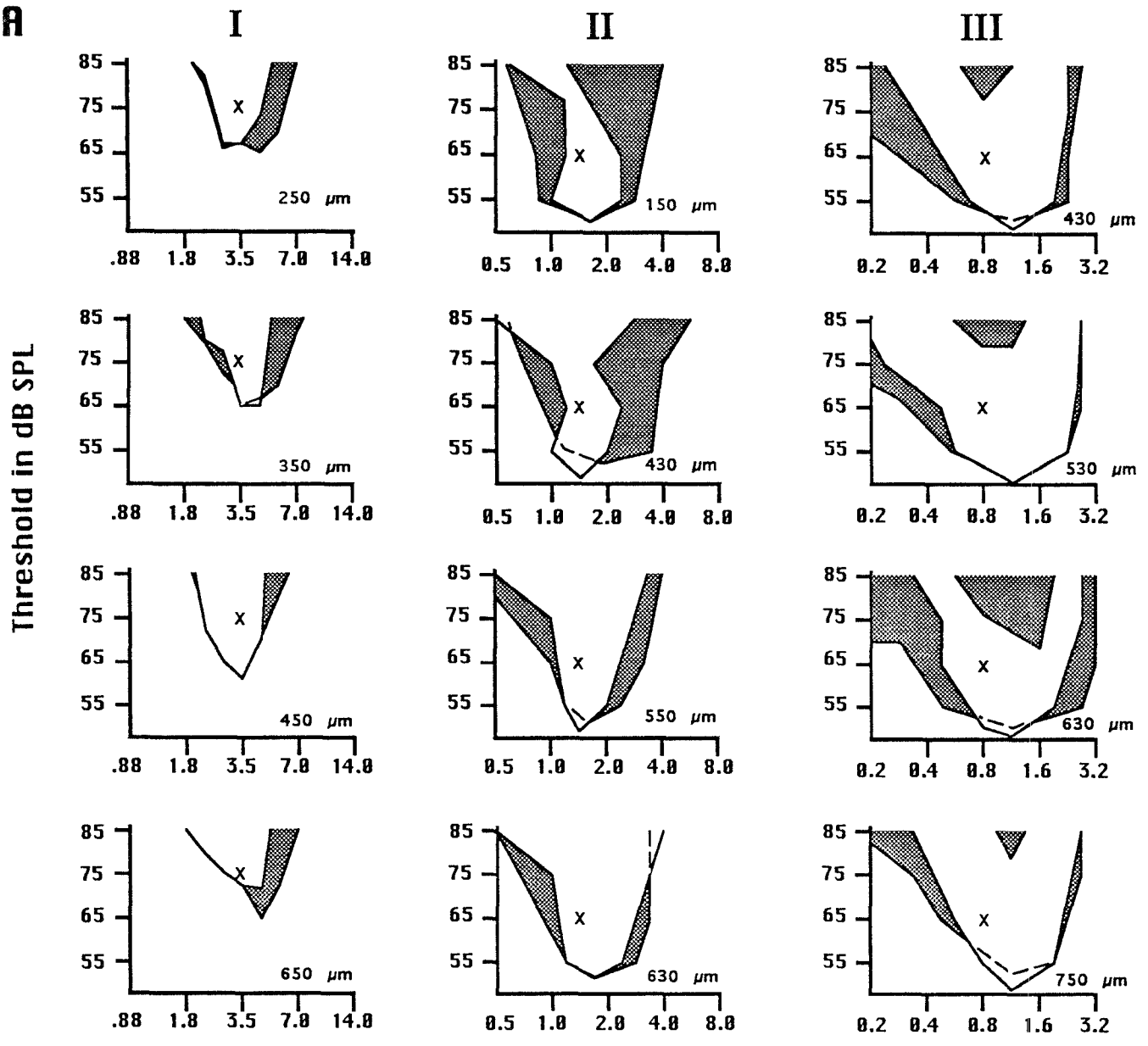
A
I
II
III
Threshold in dB SPL
85
75
65
55
250 µm
150 µm
430 µm
350 µm
430 µm
530 µm
450 µm
550 µm
630 µm
650 µm
630 µm
750 µm
.88 1.8 3.5 7.0 14.0
0.5 1.0 2.0 4.0 8.0
0.2 0.4 0.8 1.6 3.2
Frequency in kHz

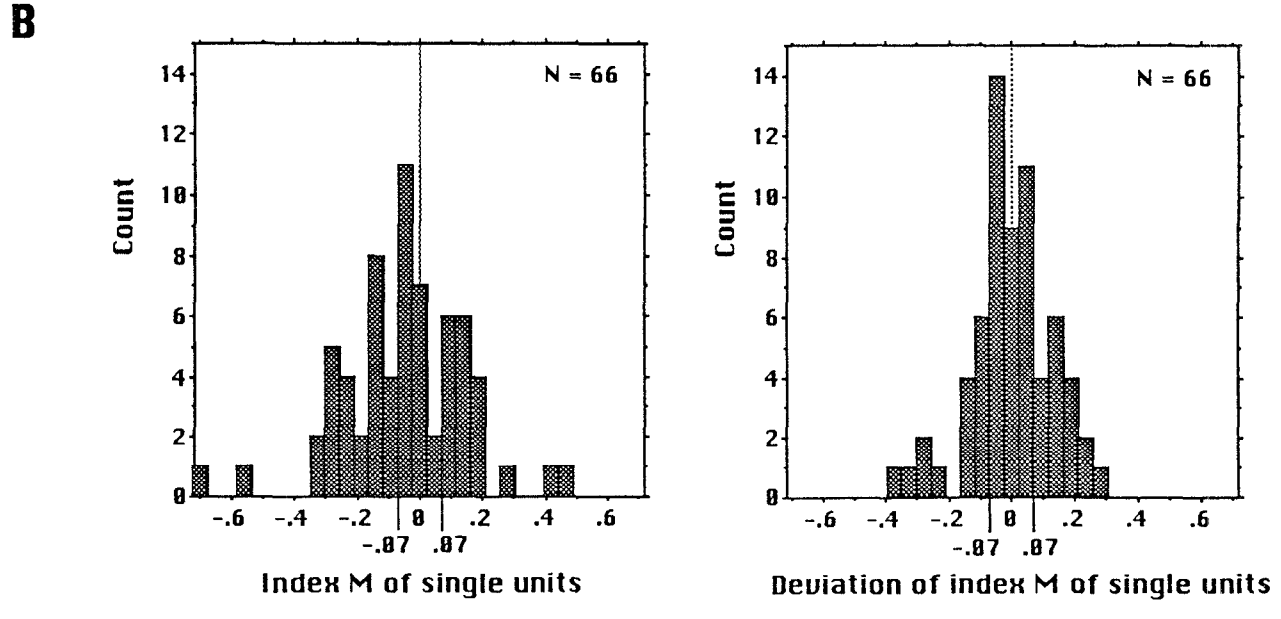
B
N = 66
Count
14
12
10
8
6
4
2
0
-.6 -.4 -.2 0 .2 .4 .6
-.07 .07
Index M of single units
Deviation of index M of single units

A

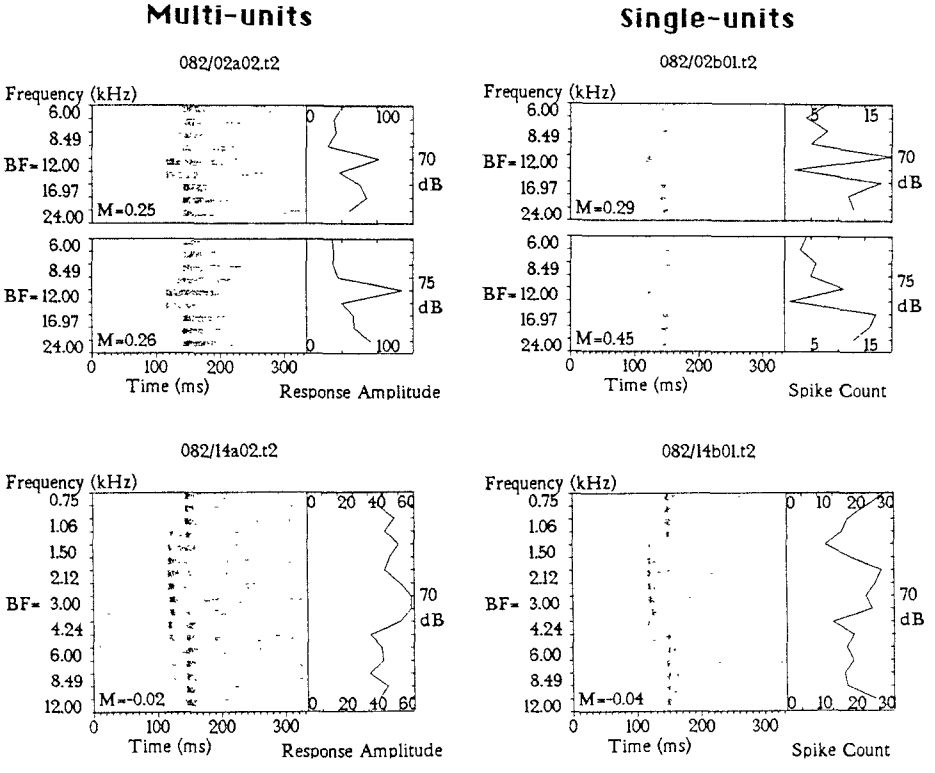
Multi-units
Single-units
082/02a02.t2
082/02b01.t2
082/14a02.t2
082/14b01.t2
Frequency (kHz)
BF= 12.00
BF= 3.00
M=0.25
M=0.26
M=0.29
M=0.45
M=-0.02
M=-0.04
70 dB
75 dB
Time (ms)
Response Amplitude
Spike Count

B

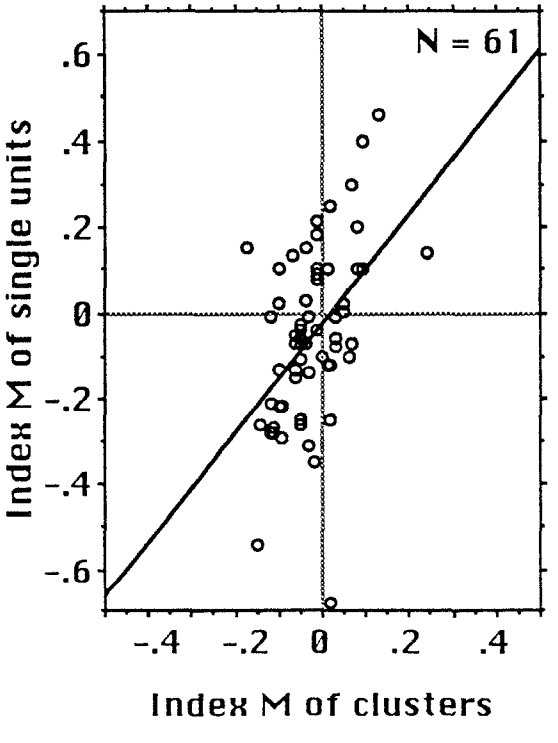
N = 61
Index M of single units
Index M of clusters
.6
.4
.2
0
-.2
-.4
-.6

Fig 7

A

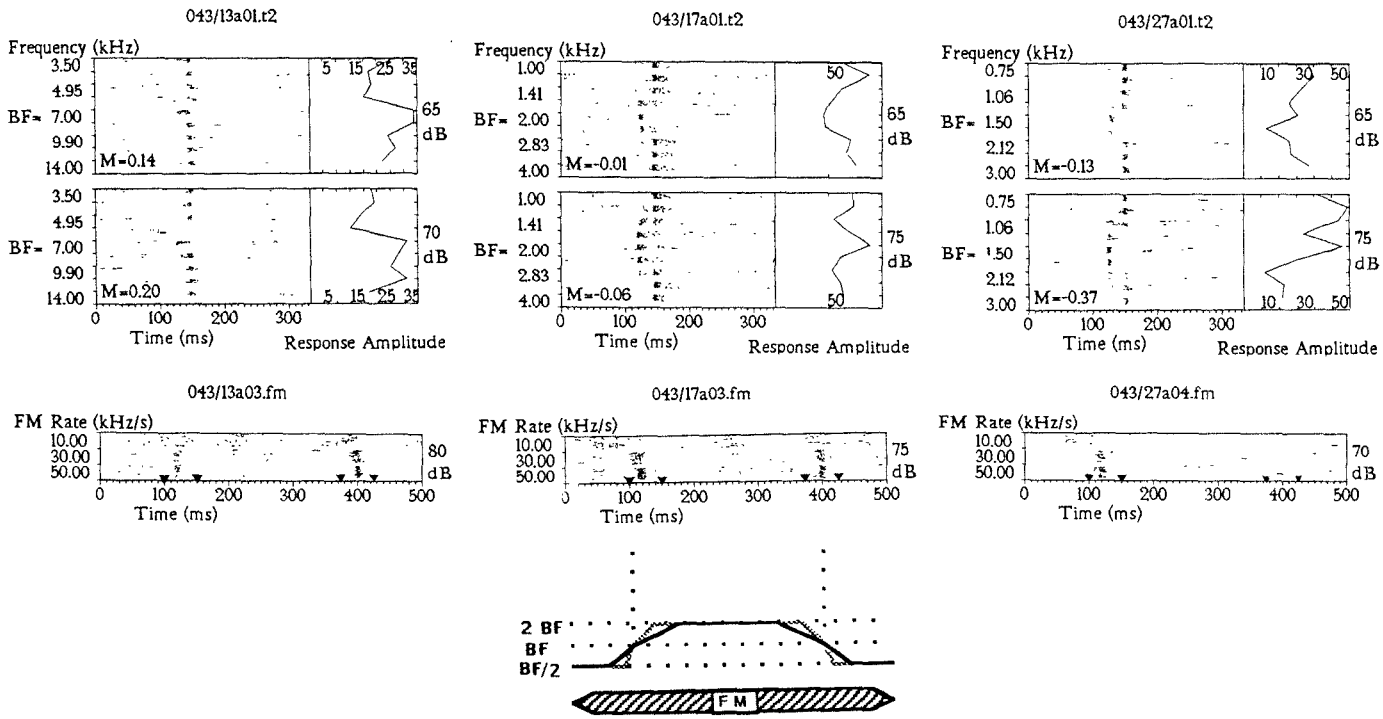
043/13a01.t2
Frequency (kHz)
3.50
4.95
BF= 7.00
9.90
14.00
M=0.14
5 15 25 35
65 dB
M=0.20
70 dB
0 100 200 300
Time (ms)
Response Amplitude
043/17a01.t2
1.00
1.41
BF= 2.00
2.83
4.00
M=-0.01
50
65 dB
M=-0.06
75 dB
043/27a01.t2
0.75
1.06
BF= 1.50
2.12
3.00
M=-0.13
10 30 50
65 dB
M=-0.37
75 dB
043/13a03.fm
FM Rate (kHz/s)
10.00
30.00
50.00
80 dB
0 100 200 300 400 500
Time (ms)
043/17a03.fm
75 dB
043/27a04.fm
70 dB
2 BF
BF
BF/2
FM

B

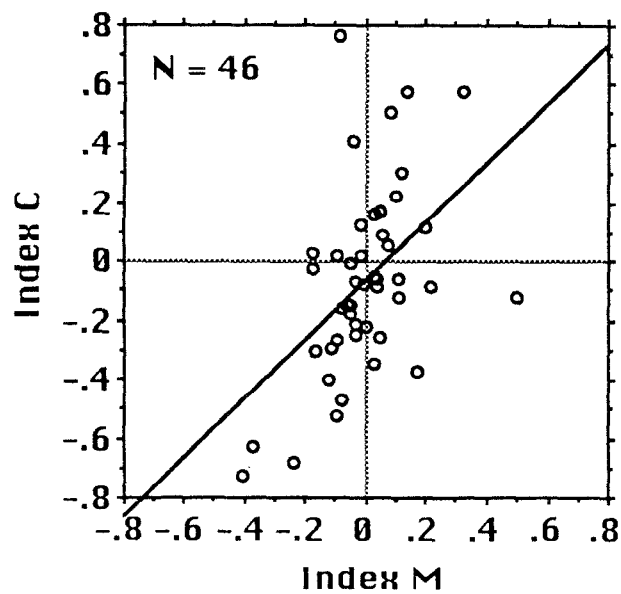
N = 46
Index C
Index M
.8
.6
.4
.2
0
-.2
-.4
-.6
-.8
-.8 -.6 -.4 -.2 0 .2 .4 .6 .8

Fig 8

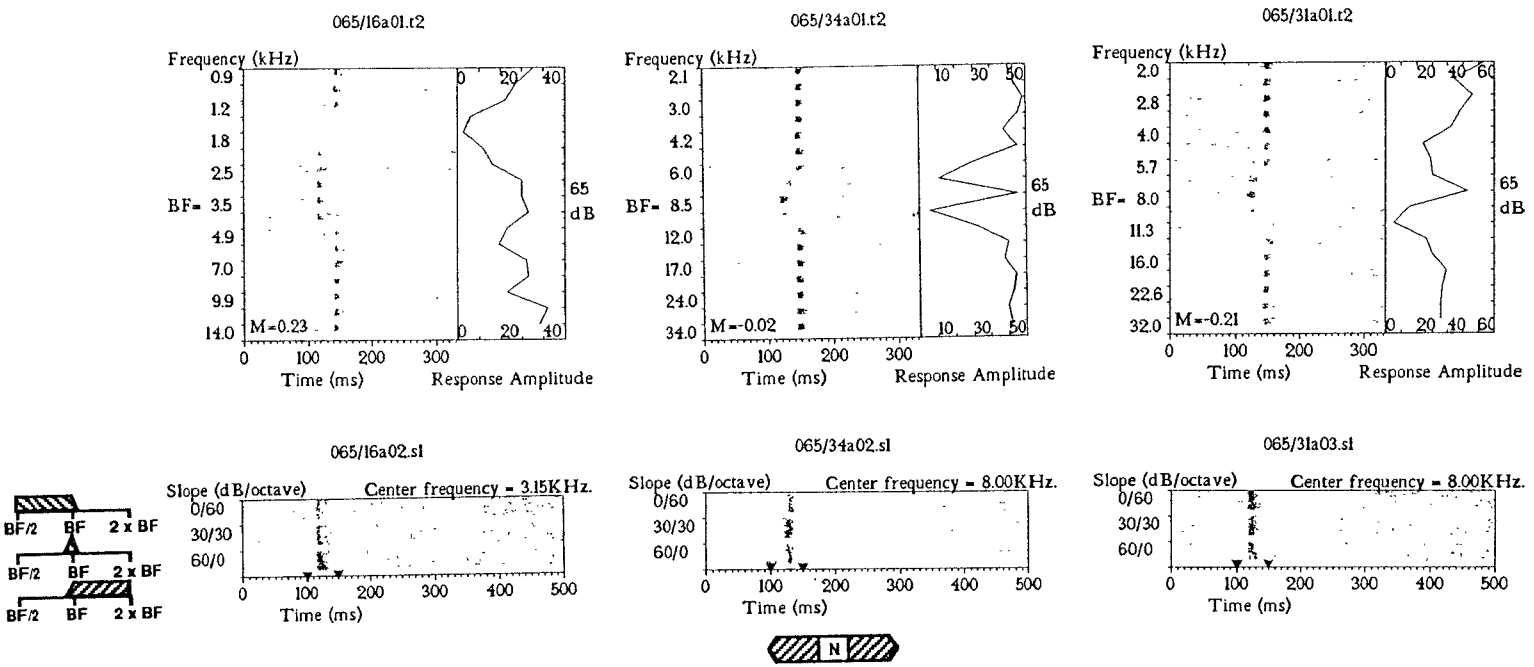
065/16a01.t2
Frequency (kHz)
0.9
1.2
1.8
2.5
BF= 3.5
4.9
7.0
9.9
14.0
M=0.23
0 20 40
65 dB
0 100 200 300
Time (ms)
Response Amplitude
065/34a01.t2
Frequency (kHz)
2.1
3.0
4.2
6.0
BF= 8.5
12.0
17.0
24.0
34.0
M=-0.02
10 30 50
65 dB
0 100 200 300
Time (ms)
Response Amplitude
065/31a01.t2
Frequency (kHz)
2.0
2.8
4.0
5.7
BF= 8.0
11.3
16.0
22.6
32.0
M=-0.21
0 20 40 60
65 dB
0 100 200 300
Time (ms)
Response Amplitude
BF/2 BF 2 x BF
BF/2 BF 2 x BF
BF/2 BF 2 x BF
065/16a02.sl
Slope (dB/octave)
Center frequency = 3.15KHz.
0/60
30/30
60/0
0 100 200 300 400 500
Time (ms)
065/34a02.sl
Slope (dB/octave)
Center frequency = 8.00KHz.
0/60
30/30
60/0
0 100 200 300 400 500
Time (ms)
065/31a03.sl
Slope (dB/octave)
Center frequency = 8.00KHz.
0/60
30/30
60/0
0 100 200 300 400 500
Time (ms)
N

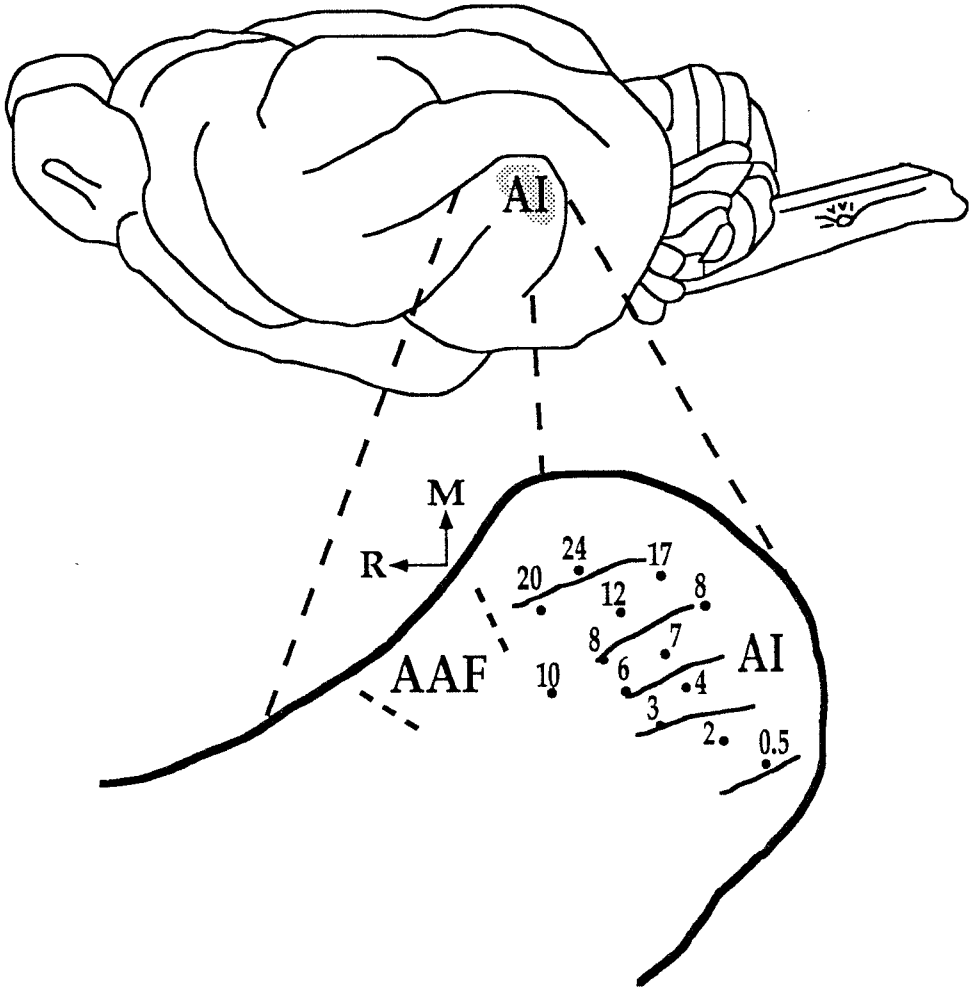
AI
M
R
24
17
20
12
8
8
7
6
4
3
2
0.5
AAF
10
AI

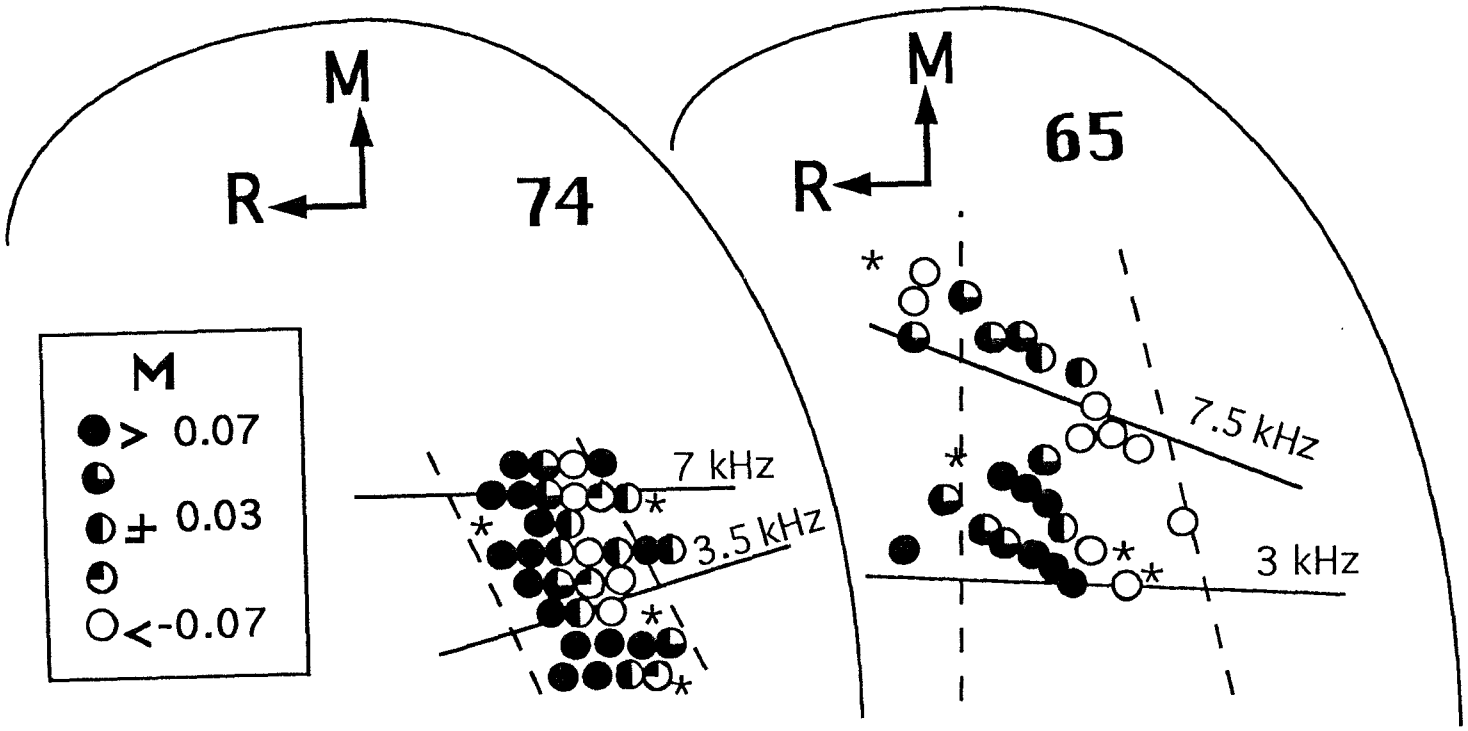
M
R
74
M
> 0.07
± 0.03
<-0.07
7 kHz
3.5 kHz
M
R
65
7.5 kHz
3 kHz

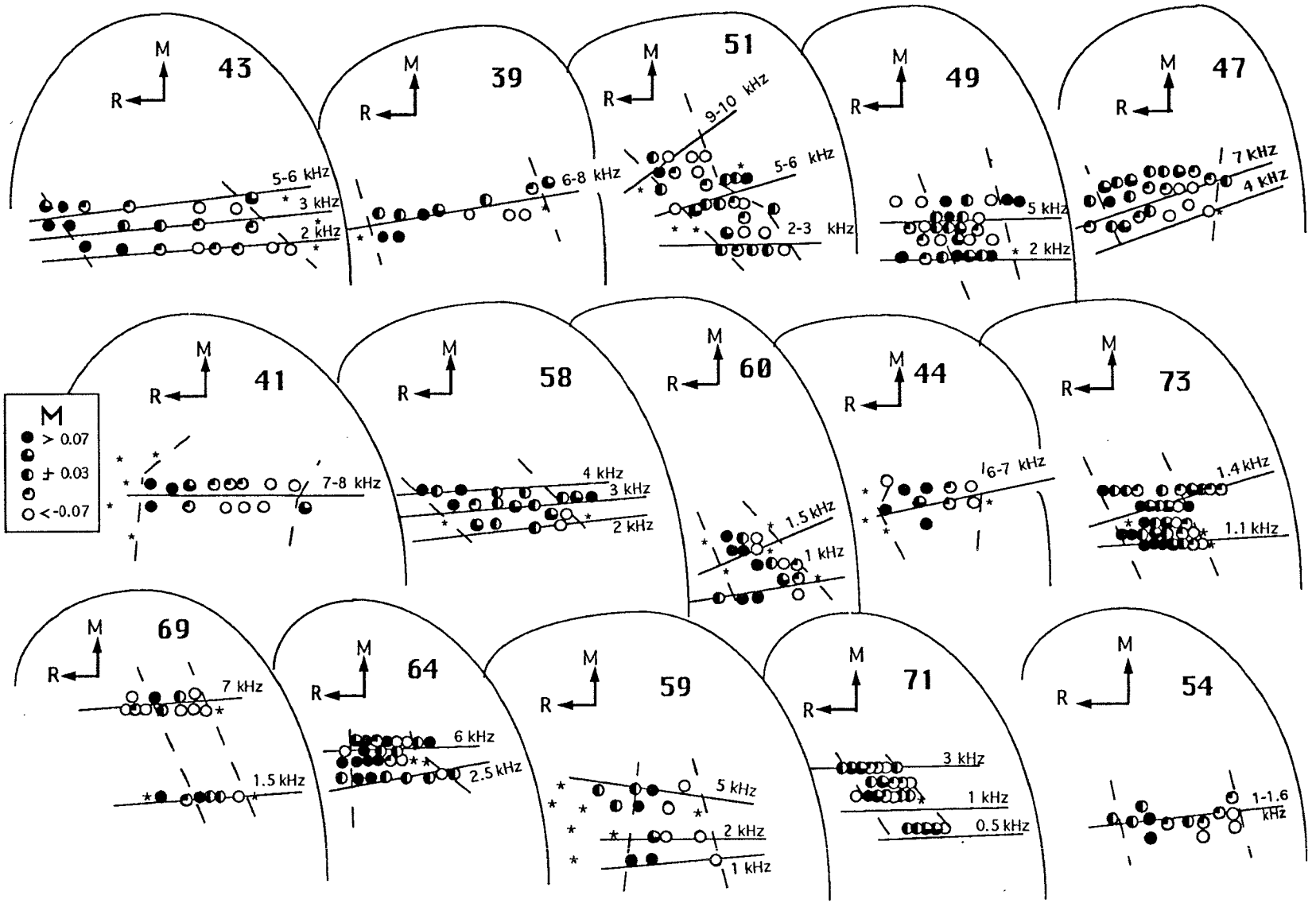
M
> 0.07
± 0.03
< -0.07
43
R
5-6 kHz
3 kHz
2 kHz
39
6-8 kHz
51
9-10 kHz
5-6 kHz
2-3 kHz
49
5 kHz
2 kHz
47
7 kHz
4 kHz
41
7-8 kHz
58
4 kHz
3 kHz
2 kHz
60
1.5 kHz
1 kHz
44
6-7 kHz
73
1.4 kHz
1.1 kHz
69
7 kHz
1.5 kHz
64
6 kHz
2.5 kHz
59
5 kHz
2 kHz
1 kHz
71
3 kHz
1 kHz
0.5 kHz
54
1-1.6 kHz

A

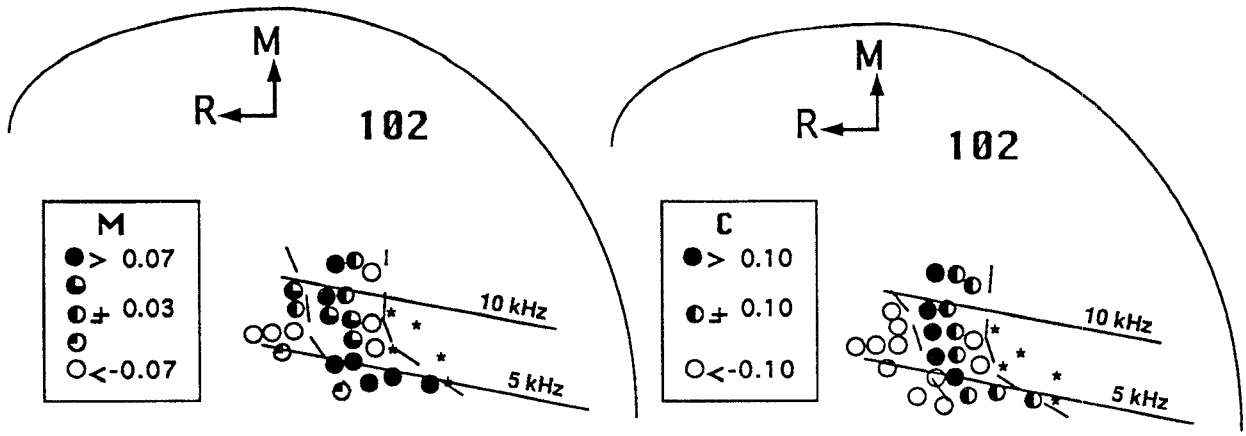
M
R
102
M
> 0.07
± 0.03
<-0.07
10 kHz
5 kHz
M
R
102
C
> 0.10
± 0.10
<-0.10
10 kHz
5 kHz

B

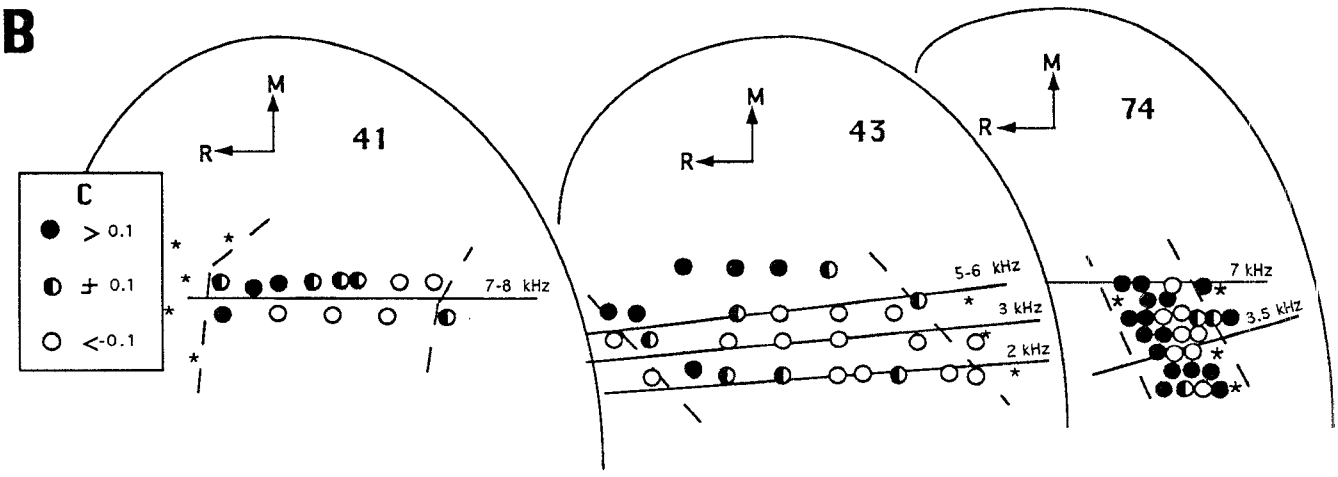
M
R
41
C
> 0.1
± 0.1
<-0.1
7-8 kHz
M
R
43
5-6 kHz
3 kHz
2 kHz
M
R
74
7 kHz
3.5 kHz

C

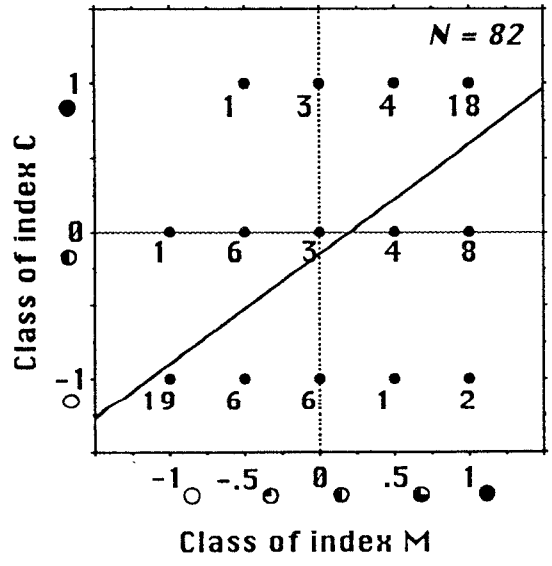
N = 82
Class of index C
1
0
-1
1 3 4 18
1 6 3 4 8
19 6 6 1 2
-1 -.5 0 .5 1
Class of index M

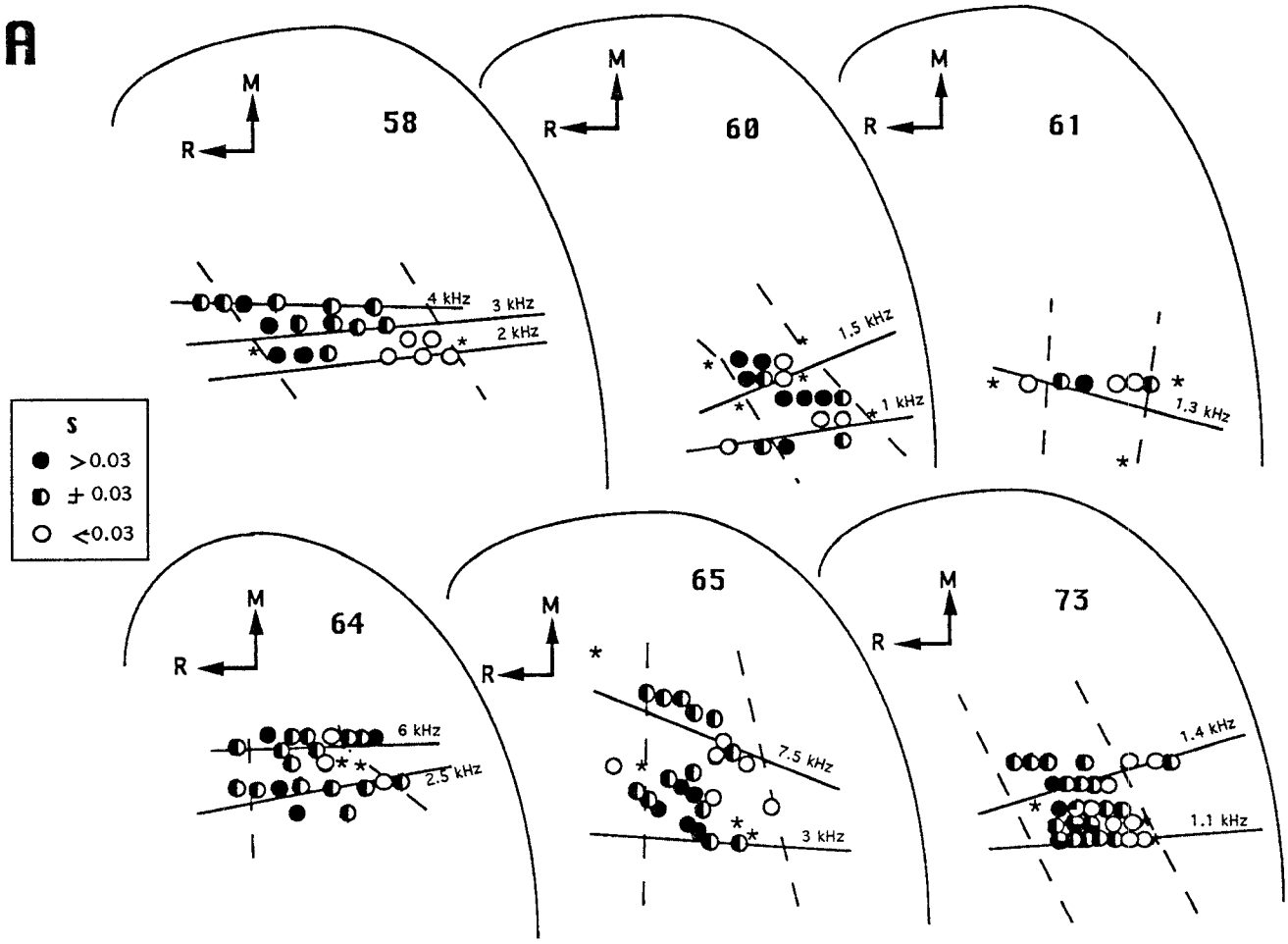
A
M
R
58
4 kHz
3 kHz
2 kHz
60
1.5 kHz
1 kHz
61
1.3 kHz
S
>0.03
± 0.03
<0.03
64
6 kHz
2.5 kHz
65
7.5 kHz
3 kHz
73
1.4 kHz
1.1 kHz

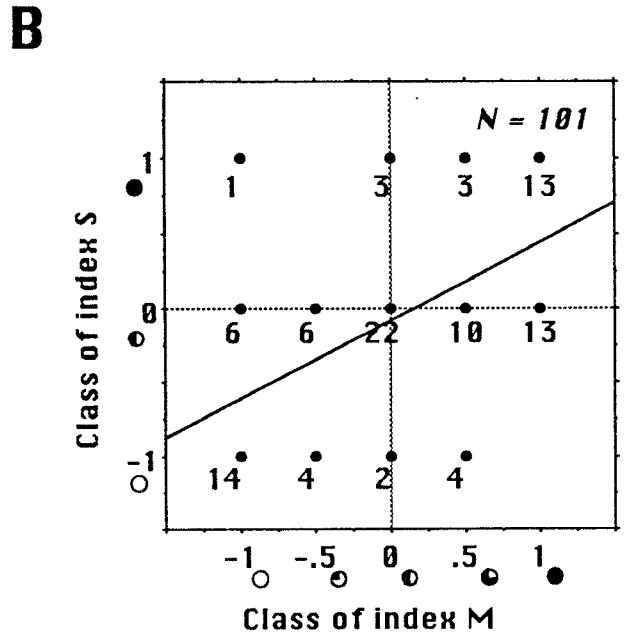
B
N = 101
1
3
3
13
6
6
22
10
13
14
4
2
4
-1
-.5
0
.5
1
Class of index S
Class of index M